Bulletin of the Geological Society of Finland, Vol. 97, 2025, pp 5–30 https://doi.org/10.17741/bgsf/97.1.001

1865 Ma tholeiitic magmatism during an extensional episode of the Svecofennian orogeny: the Kaiplot gabbros in Nagu (Nauvo), southwestern Finland

Anna E. Johnson[1]*, Olav Eklund[1] and Jussi S. Heinonen[1,2]

[1]*Geology and Mineralogy, Åbo Akademi University, Turku, Finland*
[2]*Department of Geosciences and Geography, University of Helsinki, Finland*

VERTAISARVIOITU
KOLLEGIALT GRANSKAD
PEER-REVIEWED
www.tsv.fi/tunnus

Abstract

The Svecofennian orogeny in southern Finland has traditionally been divided into two broadly defined compressional stages, the 1.89–1.87 Ga "synorogenic" stage and the ca 1.84–1.81 Ga "lateorogenic" stage. The term "intraorogenic" is used to describe a less studied stage that occurred between these two, with some overlap with both.

Mafic and intermediate intrusions collectively named as the Kaiplot gabbros are situated on a number of islands and islets in Nagu (Nauvo) in the southwestern archipelago of Finland. The outcrops occur as dykes as well as plutonic bodies and have been emplaced in at least two separate pulses. Net-veining and other structures suggesting incomplete mixing between mafic and felsic magmas are found. The main plutonic body is a hornblende gabbronorite. U-Pb dating (TIMS, zircon) gives it an age of 1865 ± 2 Ma.

Geochemically, the most primitive Kaiplot gabbros are tholeiitic and show affinity to back-arc basin basalts, indicating generation in an extensional tectonic environment. Their parental magmas appear to have originated from relatively high-degree partial melting of a shallow spinel-bearing and slightly subduction-modified depleted mantle. During transport and emplacement, both differentiation and assimilation of crustal material have taken place. The Kaiplot gabbros endorse an extensional tectonic episode of the Svecofennian orogeny at around 1865 Ma, possibly as a result of tectonic switching propagating southwestwards.

Keywords: mafic magmatism, Svecofennian orogeny, tholeiitic, geochemistry, zircon U-Pb age, Nagu, Nauvo, SW Finland, extensional tectonics.

*Corresponding author (email: anna.johnson@abo.fi)

Editorial handling: Arto Luttinen (email: arto.luttinen@helsinki.fi)

1. Introduction

When studying modern day plate tectonics, it is relatively easy to distinguish plate motions and boundaries, and where magmatism occurs. Dealing with a Proterozoic orogeny like the Svecofennian orogeny, which happened almost 2 billion years ago, is much less straightforward. The tectonic puzzle includes several orogenic stages, prolonged magmatism and periodic tectonically stable stages and the studied rocks represent a mid-crustal section of the ancient orogen.

In relation to the Svecofennian orogeny, two major compressional stages have traditionally been defined in southern Finland: the "synorogenic" (from 1.89 to 1.87 Ga), and the "lateorogenic" (from 1.84 to ca 1.81 Ga) stages (Simonen 1980; Suominen 1991; Korja & Heikkinen 2005). In the most recent recommendation of time-stratigraphic division (Kohonen et al. 2024), these stages overlap with the Middle Svecofennian (1900–1860 Ma) and the Upper Svecofennian (1860–1800 Ma). During the last 20 years, an increasing number of mafic intrusions that temporally fall between the two compressional stages have been identified. This loosely defined period of magmatism is called the "intraorogenic" stage (Simonen 1980; Nironen 2017), and the identified mantle-derived magma types vary from calc-alkaline and shoshonitic to tholeiitic N-MORB, E-MORB and OIB, and show affinities with both island-arc magmatism and extensional environments (e.g. Kara et al. 2020 and references therein). Mingling between mantle-derived mafic magmas and crust-derived felsic magmas also occur, as well as charnockitisation in the vicinity of the mafic intrusions (e.g. Konopelko & Eklund 2003; Pajunen et al. 2008). A large variety of magmas and rock types have been produced over a considerably large area during a prolonged timespan. It is not clear whether there were distinct intermittent periods between the "synorogenic, intraorogenic and lateorogenic" magmatism, or whether the magmatism was continuous.

The aim of this paper is to present the Kaiplot gabbros in Nagu (Nauvo), southwestern Finland, using petrography, age determination and geochemical methods. The gabbro intrusions will be put into a broader context of Svecofennian magmatism, and the tectonic implications that arise concerning the Svecofennian orogeny will be addressed.

2. Geological background

The study area is situated in the Southern Finland Subprovince (SFS) in the Paleoproterozoic 2.0–1.75 Ga Svecofennian domain (Gaál & Gorbatschev 1987) within the Fennoscandian Shield. The SFS (Fig. 1) is dominated by the late Svecofennian granite-migmatite (LSGM) zone (Ehlers et al. 1993). The LSGM zone is a roughly 500 km long and 100 km wide zone representing repeated strong transpressive deformation, ductile shearing and high-T low-P (amphibolite to granulite) metamorphism. The zone is characterised by extensive migmatisation and intrusions of late Svecofennian, mostly 1.84–1.81 Ga microcline granites, often porphyritic (Levin et al. 2005; Stålfors & Ehlers 2006; Skyttä & Mänttäri 2008). It overprints an area of metamorphosed volcanic and sedimentary shallow marine lithologies consisting of thin sequences of metabasalts overlain by thin layers of metamorphosed chemical sedimentary rocks comprised of marbles and iron formations. The chemical signatures of the metabasalts imply extensional rift basins (Ehlers et al. 1986). The LSGM zone covers parts of the Häme belt in the northern and the Uusimaa belt in the southern parts of SFS. In the southwest the LSGM is cut off by the 1.57 Ga Åland rapakivi massive and the South Finland shear zone (Torvela et al. 2008). When moving northwards into the Häme belt, the shallow water lithologies are less common and the chemical signatures of the basaltic lavas change to more subduction-related volcanic arc affinities (e.g. Kähkönen 2005).

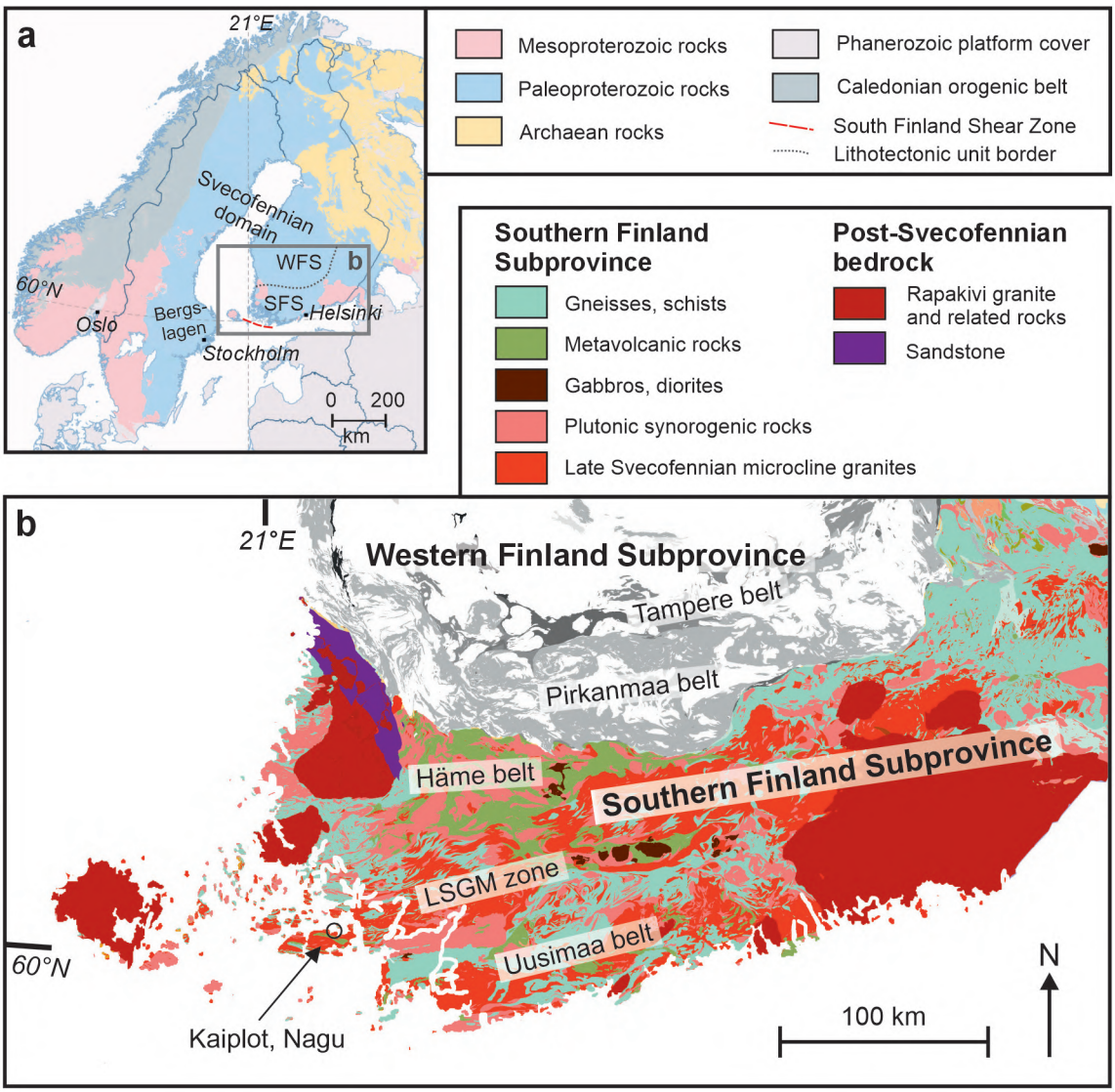

Figure 1. a) The Fennoscandian Shield, major divisions. Map modified from Koistinen et al. (2001). WFS = Western Finland Subprovince; SFS = Southern Finland Subprovince. b) Simplified geological map of Southern Finland Subprovince and its subdivisions, the location of the Kaiplot gabbros is indicated by a circle. The bedrock map is constructed using digital map information from GTK Maankamara: http://gtkdata.gtk.fi/Maankamara/index.html © Geological Survey of Finland (2016, GTK Basic licence version 1.1), Bedrock of Finland 1:200 000 (2023–2024), CC-BY-4.0.

2.1 Tectonic models

In Finland, the Svecofennian domain has traditionally been considered an accretionary orogen consisting of a series of island arcs and microcontinents that were accreted against each other and towards the Archean craton in the northeast. Age data indicate that the tectonic events become successively younger towards the southwest (e.g. Lahtinen et al. 2005; Stephens & Andersson 2015; Stephens 2020). This plate tectonic model was first suggested by Hietanen (1975)

and later developed by others (Simonen 1980; Gaál & Gorbatschev 1987; Lahtinen et al. 2005; Bogdanova et al. 2015; Nironen 2017; Lahtinen et al. 2023).

In the light of the overall model, the Svecofennian orogeny in southern Finland has been divided into the following stages: 1) the "preorogenic" stage with island arc magmatism and seafloor sedimentation (Nironen 2005); 2) the "synorogenic", main collisional stage 1.89–1.87 Ga (Väisänen et al. 2002; Lahtinen et al. 2005); 3) the "lateorogenic" compressional-transpressional stage from 1.84 to ca 1.81 Ga with high-grade metamorphism and crustal melting (Ehlers et al. 1993; Lahtinen et al. 2005; Stålfors & Ehlers 2006; Stephens & Andersson 2015); and 4) the "postorogenic" stage from ca 1.81 to 1.79 Ga with small-volume magmatism from enriched sources (Eklund et al. 1998; Rutanen et al. 2011).

However, Lahtinen & Nironen (2010) point out that the tectonic evolution of southern Fennoscandia is not compatible with merely an accretion-type model. Formation of paleosols and ultramature quartzites, both aeolian and in shallow marine basins with simultaneous magmatism at deeper crustal levels, suddenly transitioning to mass flow deposits and more immature sediments and subsequent rift-related igneous activity, indicate a gradual development from a stable intracratonic setting to an active rifting environment (Bergman et al. 2008; Lahtinen & Nironen 2010).

An alternative tectonic model was presented by Hermansson et al. (2008), in which the need for several island arcs or microcontinents is omitted by introducing a single subduction zone with constant polarity towards the northeast but with alternating net movement direction. This process called *tectonic switching* (Collins 2002) efficiently produces new continental crust by alternating cycles of compressional and extensional regimes. Hot, short-lived narrow orogenic belts form during inversion of extensional basins, and these terrains can often misleadingly be interpreted as volcanic arcs or microcontinents.

2.2 Extensional mantle-derived magmatism during the Svecofennian orogeny

An extensional stage between the two compressional stages was identified already in the beginning of the 20th Century (Ramsay 1912; Sederholm 1926) and was named "intraorogenic" by Simonen (1980), but it has often been sidelined in discussions about the Svecofennian orogeny. An increasing number of reports show that mantle-derived mafic magmatism is common in the SFS between 1870 and 1840 Ma (Suominen 1991; Lahtinen et al. 2005; Pajunen et al. 2008; Väisänen et al. 2012; Nevalainen et al. 2014; Kara et al. 2020 and others). U-Pb (zircon, monazite, titanite) dating of the intrusions give ages that span from ca 1.87 to ca 1.83 Ga with the majority so far towards the older end. Geochemically, they cover a spectrum from tholeiitic to calc-alkaline (meta-) basalts and gabbros. Both extension-related and more subduction/arc-like geochemical affinities are found. Most of the magmas were emplaced as dykes, but plutonic rocks that usually exhibit bimodal mingling structures are also found. They have been metamorphosed and deformed during the "lateorogenic" stage. Similar rock types and ages have also been recognized in the Bergslagen area in south-central Sweden (Dahlin et al. 2014; Högdahl & Bergman 2020; Johansson & Karlsson 2020) and as far east as the Ladoga region (Konopelko & Eklund 2003).

2.3 Geology of the study area

The study area is situated in the middle of the westernmost part of the LSGM zone in southern Finland (Fig. 1). The studied rocks are exposed on several islands just north of the main harbour in the central village of the former Nagu municipality in the archipelago of southwestern Finland (Fig. 2). The Pargas-Nagu-Korpo area has been affected by both the "synorogenic" and the "lateorogenic" compressional events and is now dominated by late Svecofennian granites and migmatites and

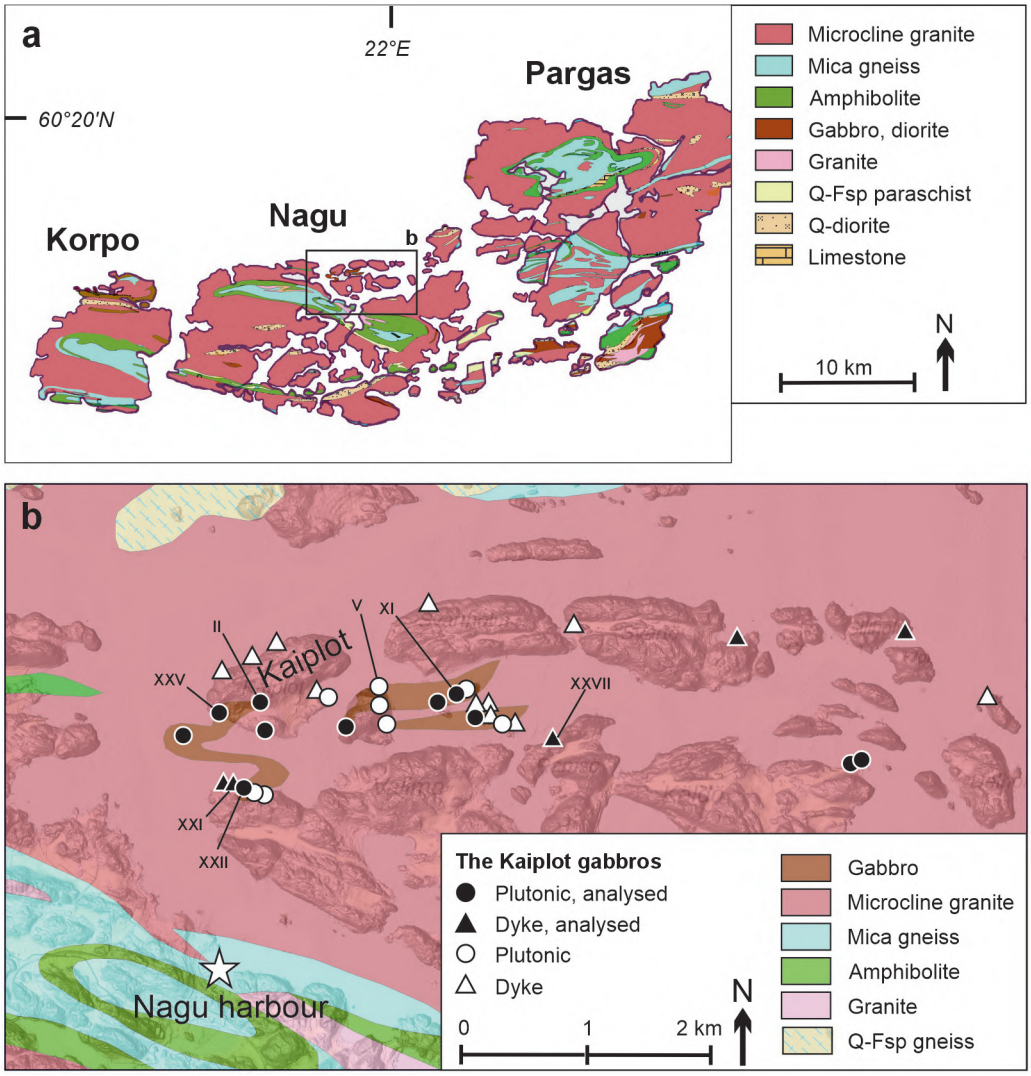

Figure 2. a) Simplified geological map of the Pargas-Nagu-Korpo area with the study area marked. b) The study area with observation and sampling points indicated. The marked outcrop numbers are referred to in the text. Coordinates for Nagu harbour: N = 6683907, E = 218035 (ETRS-TM35FIN). The bedrock map in a) and b) is constructed using digital map information from GTK Maankamara: http://gtkdata.gtk.fi/Maankamara/index.html © Geological Survey of Finland (2016, GTK Basic licence version 1.1), Bedrock of Finland 1:200 000 (2023–2024), CC-BY-4.0.

large recumbent fold-structures. The bedrock map of the area was published by Edelman (1973). In the map explanation (Edelman 1985), it is stated that the Nagu main islands are characterised by a flat oblong syncline (Fig. 2a), stratigraphically composed of, from bottom to top, 1) quartz-feldspar gneisses stemmed from psammitic shallow-water sedimentary rocks, 2) intermediate to mafic amphibolites representing basaltic to andesitic volcanic ash deposits or lavas; pillow-structures are locally preserved and the amphibolites include banded gabbros in the lowermost parts, and 3) garnet-cordierite-sillimanite mica gneisses, interpreted as deep sea clays and greywackes originally. Marbles occur as thin lenses in the quartz-feldspar gneiss, and as thicker layers in the

amphibolite and between the amphibolite and the mica gneiss (Edelman & Jaanus-Järkkälä 1983; Edelman 1985). The syncline is surrounded by a red, coarse-grained, porphyritic microcline granite that contains banded domains/parts. Hausen (1944) describes the different porphyritic granite types of the Nagu area, of which the "Mattnäs granite" in the southern part of Nagu has an ambiguous U-Pb (zircon, monazite) age of 1842 ± 31 Ma (Suominen 1991). The gabbroic rocks in the Kaiplot area were petrographically described by Hausen (1944) and commented further by Edelman (1972).

The rocks of the area have undergone metamorphosis in amphibolite to granulite facies, the maximum metamorphic temperature and pressure range during that event is estimated to have been around 800–850°C and 4–6 kbars (400–600 MPa), respectively (Väisänen & Hölttä 1999), the metamorphic grade increasing eastwards in the Nagu area (Edelman 1985). These P-T conditions correspond to a crustal depth of about 15–20 km.

3. Research materials and analytical methods

During fieldwork, 18 samples varying between 1.6 and 7 kg of the Kaiplot mafic rocks were collected for the purpose of petrographic and geochemical analysis as well as U-Pb age determination. The sampled localities are shown in Figure 2b. We sampled both plutonic rocks and dykes, avoiding visible cumulates and aimed to sample the most representative parts of the outcrops. All samples were prepared at the department of Geology and Mineralogy at Åbo Akademi University. They were first cut and crushed, and then the freshest chips were hand-picked for pulverisation. The instruments were thoroughly cleaned between samples to avoid contamination. The crushing device was a Fritsch Pulverisette jaw crusher, and the chips were ground in a ring and disc mill made of mild steel (Outokumpu brand). The risk of contamination is greatest concerning Fe, possibly up to 0.8 % (S. Fröjdö pers. comm.).

Seven thin sections from five of the outcrops (II-6, VII-9, XI-11, XXI-16 & -19, XXV-20 & -21) were chosen for detailed petrographic studies. The outcrops were selected to represent the mineralogical and geochemical variation of the area.

For the U-Pb age determinations, we chose samples II-6 and XI-11 due to their high Zr contents. The zircons were separated from the crushed samples using panning, heavy liquids and the magnetic separator Frantz. The zircons were then handpicked under a microscope and mounted in an epoxy puck. The analysis was done by Irmeli Mänttäri at the Geological Survey of Finland. The decomposition of zircon and extraction of U and Pb for multigrain TIMS (thermal ionisation mass spectrometry) isotopic age determinations mainly follow the procedure described by Krogh (1973, 1982). ^{235}U- ^{208}Pb-spiked and unspiked isotopic ratios were measured using a VG Sector 54 thermal ionization multi-collector mass spectrometer. Based on multiple analyses of SRM 981 standard the measured lead isotopic ratios were corrected for fractionation (0.10 ± 0.05 % / a.m.u.). Pb/U ratios were calculated using the PbDat-program (Ludwig 1991). Plotting of the isotopic data and final age calculation was done using the Isoplot/Ex 3 program (Ludwig 2003). All the ages are calculated at 2σ with decay constant errors ignored.

Pulverised material from all of the 18 samples were sent to Activation laboratories Ltd, Ontario, Canada (2006) for geochemical whole-rock analysis. The major elements plus Sc, Be, V, Sr, Zr and Ba were analysed by FUS-ICP (Fusion-Inductively Coupled Plasma Optical Emission Spectroscopy), and the minor and trace elements (e.g. REE) were analysed by FUS-MS (Fusion-Mass Spectrometry). The whole-rock analysis data is presented in Table 1. Concentrations for Be, As, Mo, Ag, In, Sn, Sb, W, Tl, Pb, and Bi were below or so close to detection limit in general that they are not reported here. Based on analysis of standard materials compositionally similar to our samples, the maximum offset from recommended value (accuracy) for major element oxides is considered to be ≤ 3 %, except ≤ 5 % for Na_2O and about ≤ 10 %

for P_2O_5. Based on duplicate analysis of our sample and a standard sample that was analysed at about the same time (D'Elia 2010), the coefficient of variation (precision) is ≤ 2 % for all major element oxides, except for K_2O and P_2O_5 (≤ 5 %). The limits of detection for Cr, Ni, Cu and Zn are quite high with FUS-MS (<10–30 ppm), so their concentrations have been rounded to the nearest ten. The offset and coefficient of variation for them are considered to be less than 10–20 % in general. For other trace elements, the offset and coefficient of variation are generally less than 10 %, but can be higher for some (e.g., Ge, Nb, Sb, La, Ce, Pr, Ta, U and Th), especially if their concentrations are close to the respective detection limits. Standard and duplicate analyses and more detailed information about accuracy and precision can be found in Electronic Appendix A.

Thin section XXV-20 was studied with a Phenom XL Desktop SEM (Thermo Fisher Scientific Inc, Phenom-World B.V., Dillenburgstraat 9T, 5652 AM Eindhoven, The Netherlands). The electron source is a CeB_6 crystal, and samples can be imaged with a four-segment backscattered electron detector (BSD) under a variable vacuum and no carbon coating is needed. For semi-quantitative mineral analysis, the thin section was carbon coated, and data were collected with the integrated energy-dispersive X-ray spectroscopy detector (EDS; thermoelectrically cooled 25 mm^2 Silicon Drift Detector with an ultra-thin Si_3N_4 window). Data reduction and ZAF correction was performed with the proprietary software (Phenom Pro Suite). The SEM data is found in Electronic Appendix A.

4. Results

4.1 Field observations and petrography

Most of the mafic outcrops are relatively flat surfaces by the water where waves and ice keep the shorelines clean from moss and lichen. The mafic rocks in the study area occur as both dyke-like intrusions and larger bodies (Fig. 2 and 3). The largest exposed plutonic body is situated mainly on the island of Kaiplot extending to the smaller islets east of Kaiplot, and we chose the name *Kaiplot gabbros* to represent all the mafic rocks of the study area, including rocks that are not (necessarily) geochemically classified as gabbros.

The main plutonic body exhibits a variety of grain sizes from fine-grained (0.1–1 mm) to coarse-grained (1–10 mm). Most of the larger bodies are medium-grained and massive, but in places they contain narrow bands with different mineral proportions, or structures that resemble flow banding (e.g. Fig. 3b). On most outcrops, the gabbros are clearly foliated in the same direction as the surrounding porphyritic granites. On outcrop XXV, two emplacement pulses can be distinguished. Here a massive medium-grained rock (XXV-21) and a fine-grained banded rock (XXV-20) lie side by side with inclusions of the first inside the latter (Fig. 3a, b). These fragments have sharp edges as if brecciated. On other outcrops, irregular quenched enclaves with rounded outlines are found, possibly representing autoliths or cumulates. The contacts between the mafic plutonic rocks and the surrounding granites are not exposed.

The thin section study of the largest plutonic body reveals that the main minerals are plagioclase (~An_{50} based on the Michel-Levy method) and pleochroic amphibole in different shades of green to brown. The more primitive samples contain abundant ortho- and clinopyroxene, and ilmenite as a minor phase. SEM analysis of one of the most primitive samples (XXV-20: Fig. 3b and 4a, b) shows the orthopyroxene to be En_{50} and the clinopyroxene to be augite. Exsolution lamellae with lower Ca-content are common in them. In the more differentiated samples, pyroxenes are highly altered to microcrystalline materials. Biotite and quartz appear as minor to main phases. Apatite is an abundant accessory mineral in the differentiated samples, and there are virtually no opaques. Orthopyroxene is variably replaced by symplectic amphibole ± opaques ± quartz ±

Table 1. Geochemical data for the Kaiplot gabbros.

Sample	I-5	II-6	VII-9	VIII-10	XI-11	XIX-37	XX-15	XXI-16	XXI-19	XXII-18	XXV-20	XXV-21	XXVII-24	XXX-36	XXXI-26	XXXII-27	XXXIV-38	XXXVI-41
N	6685996	6686200	6685969	6686255	6686306	6686191	6685570	6685568		6685557	6686117		6685997	6685751	6685770	6686839	6685958	6686793
E	218448	218532	219113	219908	220061	220205	218158	218243		218288	218124		220935	223359	223388	223808	217817	222458
Type	Plutonic	Plutonic	Plutonic	Plutonic	Plutonic	Dyke	Dyke	Dyke	Dyke	Plutonic	Plutonic	Plutonic	Dyke	Plutonic	Plutonic	Dyke	Plutonic	Dyke
Age data		1865 ± 2 Ma			1865 ± 2 Ma													
Primitive/ Differentiated	Diff.	Diff.	Diff.	Prim.	Diff.	Prim.	Prim.	Prim.	Diff.	Diff.	Prim.	Diff.	Prim.	Diff.	Prim.	Diff.	Diff.	Diff.
Element, wt.%																		
SiO_2	49.53	50.05	51.00	49.95	49.30	48.23	49.42	50.39	56.25	48.22	49.13	50.93	49.85	49.39	49.41	49.51	52.39	55.44
TiO_2	2.90	3.18	1.58	0.98	2.49	1.66	1.57	1.28	0.85	1.68	1.66	1.56	0.94	2.52	2.75	1.99	1.29	1.09
Al_2O_3	18.56	18.61	19.04	17.32	17.93	17.41	13.38	13.54	14.25	18.15	14.23	20.27	13.35	16.83	16.76	18.38	16.01	19.47
Fe_2O_3(T)	10.22	10.60	8.01	10.33	11.48	11.65	14.13	13.36	11.79	9.89	11.98	7.92	11.36	13.32	11.21	10.25	10.91	7.78
MnO	0.12	0.12	0.10	0.15	0.11	0.15	0.20	0.19	0.14	0.12	0.18	0.09	0.18	0.17	0.14	0.14	0.15	0.05
MgO	3.60	3.73	5.37	7.66	3.41	5.87	7.27	7.60	4.28	6.43	7.69	3.47	9.66	4.31	5.43	4.74	5.81	2.46
CaO	10.10	8.85	9.04	10.53	9.25	9.90	10.71	10.09	8.13	11.07	11.50	10.53	11.82	9.38	9.05	10.41	7.99	6.87
Na_2O	3.67	3.77	3.35	2.52	3.54	2.83	2.43	2.12	2.52	2.61	2.70	3.73	2.03	3.19	3.40	3.17	3.03	3.32
K_2O	0.70	0.76	1.13	0.46	1.04	1.01	0.47	0.85	0.76	1.15	0.64	0.79	0.43	0.52	0.99	0.50	1.27	1.21
P_2O_5	0.14	0.17	0.16	0.07	0.21	0.15	0.15	0.09	0.19	0.03	0.13	0.15	0.06	0.27	0.12	0.24	0.20	0.29
LOI	0.73	0.37	1.51	0.31	1.45	1.03	0.53	0.83	0.94	0.95	0.20	0.79	0.50	0.01	1.14	0.22	0.57	1.94
Total	100.30	100.20	100.30	100.30	100.20	99.89	100.30	100.30	100.10	100.30	100.00	100.20	100.20	99.81	100.40	99.54	99.62	99.92
Mg#	41.10	41.08	57.05	59.50	37.05	49.96	50.48	52.99	41.83	56.29	55.98	46.47	62.75	39.06	48.97	47.81	51.34	38.52
Element, ppm																		
Sc	18	20	16	28	27	31	40	37	31	23	41	17	41	32	22	20	29	23
V	299	214	128	191	268	235	315	269	208	219	250	151	238	285	298	193	193	102
Cr	b.d.l.	50	160	80	50	b.d.l.	110	150	40	230	260	70	250	b.d.l.	160	100	180	b.d.l.
Co	36	32	28	45	41	34	58	54	36	43	45	28	50	35	37	29	32	15
Ni	40	30	70	20	30	b.d.l.	50	50	b.d.l.	50	b.d.l.	30	70	b.d.l.	50	30	40	b.d.l.
Cu	190	60	30	30	300	10	130	40	50	20	20	90	10	60	90	30	90	210
Zn	100	180	90	120	160	90	100	160	110	110	120	110	110	120	200	110	120	80
Ga	33	32	30	24	31	22	26	23	22	24	22	31	20	25	30	28	22	26
Ge	1.7	1.7	1.3	1.8	1.4	2.0	1.5	2.0	1.8	1.4	2.1	1.4	1.8	2.0	1.9	1.0	2.0	1.0
Rb	18	29	46	9	37	23	11	49	28	63	8	25	11	11	60	15	64	87
Sr	334	268	291	183	294	242	139	113	184	232	191	252	136	323	263	295	269	365
Y	25.6	26.7	22.3	20.9	38.1	27.0	31.9	25.9	22.9	10.0	30.7	26.9	16.5	35.0	21.3	33.0	34.0	25.0
Zr	79	148	118	41	140	94	71	59	45	24	85	93	33	150	65	146	157	295
Nb	12.2	14.4	10.5	3.2	15.6	6.0	6.5	3.4	3.1	3.8	3.1	9.6	2.3	12.0	9.6	11.1	10.0	14.0
Cs	0.2	0.5	2.5	0.2	0.9	1.6	0.2	0.4	0.5	1.8	b.d.l.	0.4	0.3	0.5	2.7	0.6	1.1	11.6
Ba	156	148	107	69	203	150	46	58	144	88	62	86	62	175	154	149	333	346
Hf	2.8	5.1	4.1	1.7	4.7	3.0	2.6	2.2	1.8	1.1	3.0	3.5	1.4	4.3	2.4	5.0	4.6	7.3

Ta	0.91	1.10	0.59	0.18	0.87	0.40	0.46	0.23	0.13	0.31	0.19	0.60	0.12	0.80	0.77	0.79	0.60	0.90		
Th	0.45	0.77	5.31	0.27	0.80	0.50	0.92	1.44	4.06	1.26	0.54	1.31	0.35	0.60	0.76	1.20	0.50	5.80		
U	0.37	0.59	1.04	0.17	0.59	0.30	0.37	0.62	0.95	0.60	0.26	0.56	0.13	0.40	4.31	1.12	0.40	2.10		
La	14.40	16.20	22.30	5.46	21.30	9.90	10.60	8.49	15.40	6.21	7.43	14.60	4.69	14.90	11.00	20.10	16.60	24.20		
Ce	34.2	38.9	50.7	13.7	55.6	23.9	27.1	20.4	35.4	13.2	19.0	35.7	11.5	36.5	25.8	49.4	40.9	50.7		
Pr	4.66	5.35	6.49	1.86	7.92	3.09	3.78	2.72	4.54	1.67	2.86	4.71	1.63	4.87	3.45	6.66	5.51	6.15		
Nd	19.50	23.00	25.70	8.93	35.20	14.10	16.60	12.90	18.90	6.87	14.60	19.80	7.92	23.00	15.10	28.80	25.00	26.50		
Sm	5.08	6.12	5.69	2.76	9.12	3.80	4.59	3.69	4.47	1.73	4.31	4.93	2.31	6.00	3.82	7.16	6.30	5.70		
Eu	1.84	1.73	1.46	1.03	1.90	1.45	1.34	1.14	1.10	1.07	1.56	1.37	0.89	2.09	1.44	2.03	1.52	1.99		
Gd	5.01	5.86	5.05	3.22	8.81	4.50	4.92	4.08	4.26	1.91	4.96	5.04	2.73	6.70	3.99	7.31	6.40	5.70		
Tb	0.83	0.93	0.78	0.58	1.38	0.70	0.90	0.74	0.68	0.33	0.90	0.84	0.50	1.10	0.69	1.15	1.10	0.80		
Dy	4.76	5.02	4.28	3.56	7.51	4.40	5.52	4.60	4.03	1.94	5.49	4.81	3.13	6.20	3.93	6.45	6.00	4.40		
Ho	0.94	0.94	0.82	0.75	1.46	0.90	1.13	0.95	0.84	0.39	1.10	0.94	0.65	1.20	0.77	1.21	1.10	0.80		
Er	2.69	2.77	2.33	2.23	4.09	2.60	3.38	2.85	2.58	1.14	3.23	2.75	2.05	3.40	2.26	3.43	3.30	2.40		
Tm	0.38	0.39	0.34	0.33	0.56	0.39	0.49	0.42	0.39	0.17	0.48	0.40	0.31	0.50	0.32	0.51	0.49	0.36		
Yb	2.23	2.23	2.01	2.04	3.29	2.50	3.00	2.64	2.48	1.03	2.97	2.41	1.90	3.10	1.86	3.10	3.10	2.30		
Lu	0.31	0.31	0.28	0.29	0.46	0.41	0.42	0.38	0.37	0.15	0.42	0.34	0.28	0.46	0.27	0.43	0.45	0.35		

Coordinates are ETRS-TM35FIN. Mg# calculated as 100*(MgO/(FeO+MgO)) [mol.%].

biotite (uralitisation), and plagioclase is weakly altered to saussurite/sericite. Due to their mineral composition, we suggest that the Kaiplot gabbros should be classified as hornblende-gabbronorites.

In the medium-grained samples of the main plutonic body, the mafic minerals tend to form aggregates that occasionally show a preferred orientation that gives the outcrops their foliated appearances (Fig. 4c, d). The average grain size is around 1–2 mm with sporadic plagioclase and amphibole grains being up to 4 mm long, however. The fine-grained banded sample (XXV-20, Fig. 3b and 4a, b) has alternating pyroxene-rich and amphibole-rich bands that are ≤ 3 mm in thickness. The grain sizes are in general less than 0.5 mm.

The dykes have intruded both the porphyritic and the relatively even-grained granite variants. Since the dykes have been sheared together with the granites, they are now in some cases flat lying, sheared and altered, and the closest contact zones to the surrounding rock are often eroded. Their appearance in the field is nevertheless crosscutting the other lithologies. On outcrop XXI there is a dyke that has intruded in two separate pulses with different composition, but the order of the intrusions is unclear (Fig. 3c).

The thin sections from the two dykes on outcrop XXI are both fine-grained with average grain sizes of ≤ 0.5 mm. The more primitive of the dykes (XXI-16, lower in Fig. 3c) consists mostly of plagioclase, amphibole, clinopyroxene and minor opaques, but it also contains light-coloured veins of extensively altered clinopyroxenes, chloritized amphibole and quartz. The more differentiated dyke (XXI-19) is dominated by elongated amphibole grains with a preferred orientation as well as abundant quartz and biotite (Fig. 4e, f). Occasional plagioclase grains and remnants of highly altered pyroxene can be found. Accessory apatite is abundant.

The bedrock in the study area shows signs of bimodal magmatism. This is manifested as mingling structures (outcrop V, Fig. 3d) and fingering, i.e. a dyke intruding into and interrupted by a highly viscous felsic body, as well as back-veining and incomplete mixing of a mafic and a felsic magma.

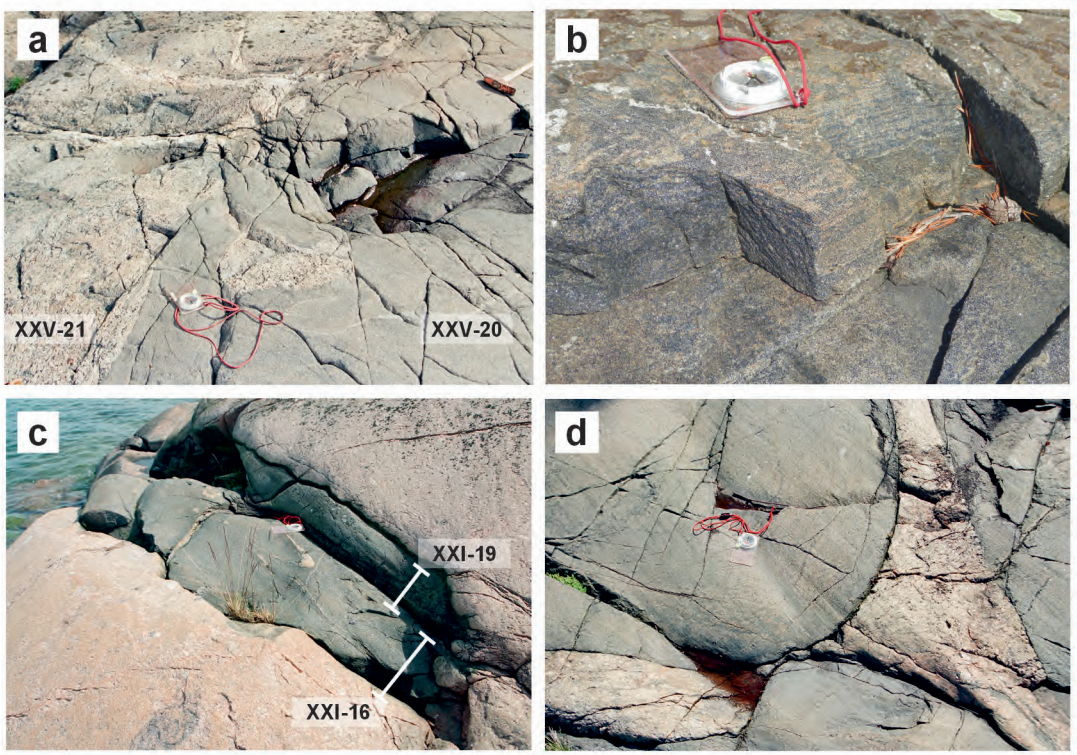

Figure 3. Field photos. a) The main plutonic body, outcrop XXV. Two emplacement pulses, both gabbroic, with different grain sizes. b) Close-up of the fine-grained banded mafic rock, XXV-20. c) Dyke intrusion, outcrop XXI. Two emplacement pulses surrounded by porphyritic granite. d) Mingling between a mafic and a felsic component, outcrop V.

Table 2. Multigrain TIMS zircon U-Pb isotopic data for the Kaiplot gabbros.

Sample information	Sample	U	Pb	$^{206}Pb/^{204}Pb$	$^{208}Pb/^{206}Pb$	ISOTOPIC RATIOS[1]						Rho[2]	APPARENT AGES / Ma±2 σ		
	mg	ppm		measured	Radiogenic	$^{206}Pb/^{238}U$	±2σ%	$^{207}Pb/^{235}U$	±2σ%	$^{207}Pb/^{206}Pb$	±2σ%		$^{206}Pb/^{238}U$	$^{207}Pb/^{235}U$	$^{207}Pb/^{206}Pb$
A#2) XI-11; Zr abraded 20 h	0.53	809	294	2278	0.15	0.3276	0.33	5.1480	0.34	0.1140	0.07	0.98	1827	1844	1864±1
B) XI-11; Zr abraded 25 h	0.50	749	272	2257	0.14	0.3286	0.33	5.1619	0.34	0.1139	0.06	0.98	1832	1846	1863±1
C) XI-11; Zr abraded 10 h	0.41	774	277	2408	0.14	0.3231	0.33	5.0768	0.34	0.1140	0.06	0.98	1805	1832	1863±1
D) II-6; Zr abraded 20 h	0.50	932	322	2853	0.13	0.3159	0.33	4.9571	0.33	0.1138	0.06	0.98	1770	1812	1861±1

1) Isotopic ratios corrected for fractionation, blank (35-50 pg), and age-related common lead (Stacey and Kramers (1975); $^{206}Pb/^{204}Pb$ ± 0.2, $^{207}Pb/^{204}Pb$ ± 0.1, $^{208}Pb/^{204}Pb$ ± 0.2).

2) Rho: Error correlation between $^{206}Pb/^{238}U$ and $^{207}Pb/^{235}U$ ratios. All errors are 2 σ.

4.2 U-Pb analysis

For the U-Pb analysis, the most transparent and inclusion-free zircon grains were selected. The zircons of the sampled Kaiplot gabbros are brownish, translucent, and elongated. They contain dark inclusions and the crystal faces are undeveloped or corroded. Three zircon fractions from sample XI-11 (A#2, B and C) and one fraction from sample II-6 (D) were analysed (Table 2), the first analysis of fraction A failed but the second was successful. The four-point discordia line intercepts the concordia curve at 1865 ± 2 Ma, which is considered the magmatic age of the Kaiplot gabbros (Fig. 5).

4.3 Geochemistry

All the 18 analysed Kaiplot gabbros (Table 1, Electronic Appendix A) fall within the igneous

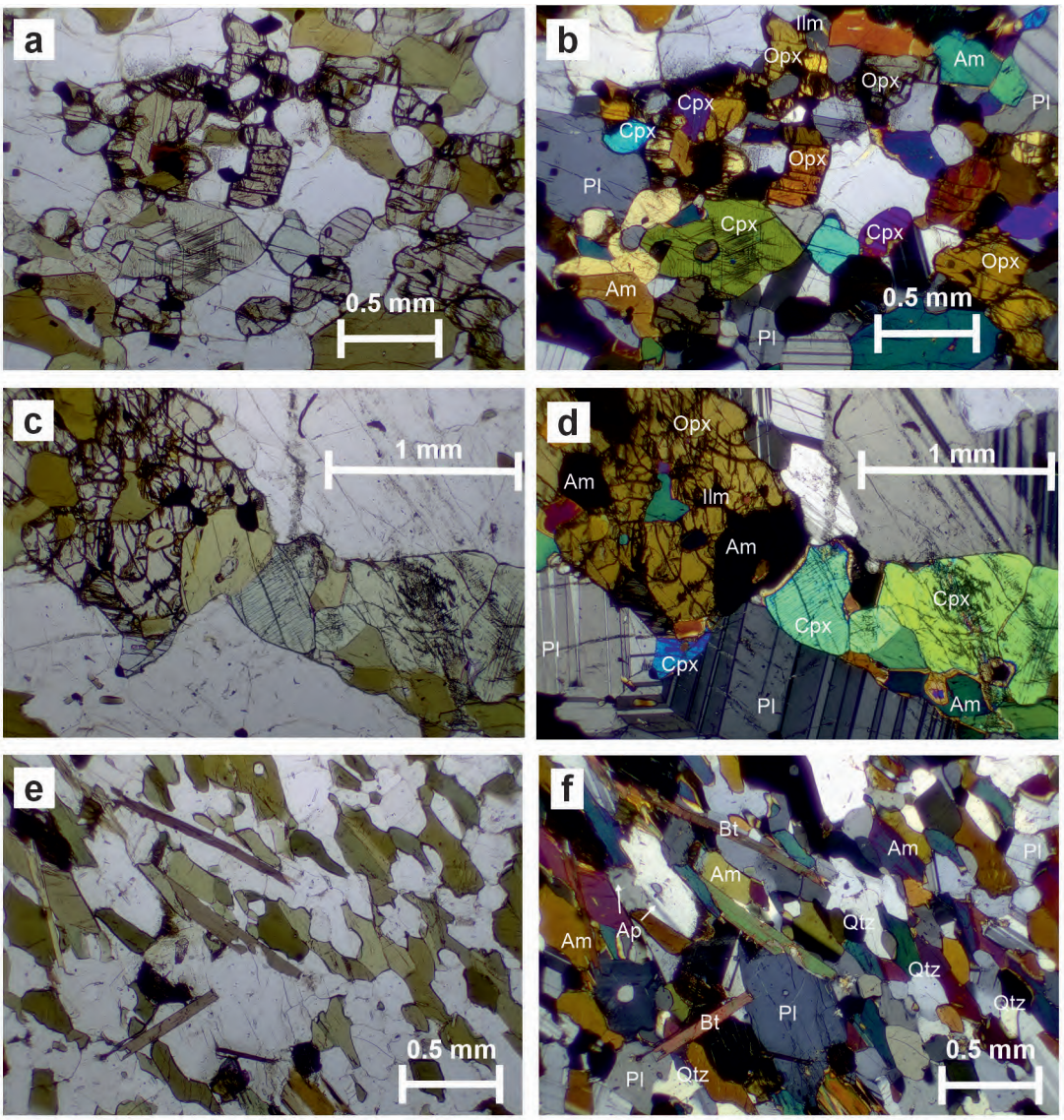

Figure 4. Photos of the thin sections, plane-polarised to the left, cross-polarised to the right. a) and b) from the main plutonic body, the fine-grained and banded XXV-20, a light pyroxene-rich band. c) and d) from outcrop II in the main plutonic body, medium-grained with mafic aggregates. e) and f) from the differentiated dyke on outcrop XXI. Am = amphibole; Opx = orthopyroxene; Cpx = clinopyroxene; Pl = plagioclase; Bt = biotite; Qtz = quartz; Ap = apatite; Ilm = ilmenite.

spectrum of Hughes (1972) and have not thus been significantly altered. The samples have SiO_2 contents ranging from 48 to 56 wt.%. and the majority fall in the 49–52 wt.% range. Total alkalis (Na_2O+K_2O) are 2.5–4.6 wt.%. Most of the samples are subalkaline and tholeiitic gabbros (Fig. 6). The Al_2O_3 contents are 13–20 wt.%, MgO 2.5–9.7 wt.%, Fe_2O_3(T) 8–14 wt.% while the TiO_2 variation is 0.8–3.2 wt.%. Magnesium numbers (Mg#) range from 37 to 63 (Table 1).

To be able to classify gabbros geochemically and investigate their tectonic origin, we have screened the data to make it possible to separate samples that deviate significantly from primitive melt compositions. The following screening criteria are used in this paper: SiO_2 = 45–52 wt.%,

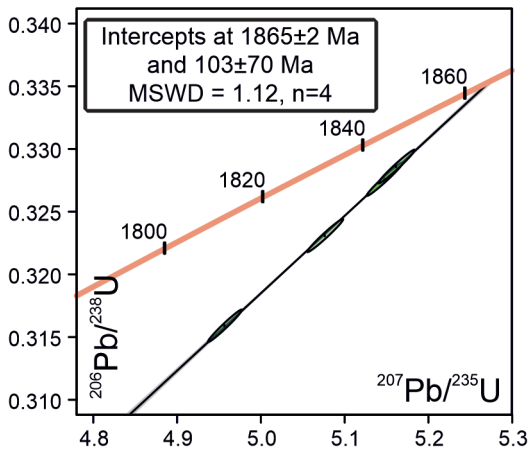

Figure 5. Concordia plot for TIMS multigrain zircon U-Pb isotopic data from the Kaiplot gabbros, samples II-6 and XI-11.

MgO = 5–12 wt.%, Al_2O_3 < 18 wt.%, Ni < 200 ppm and Cr < 600 ppm. These criteria help to select basaltic samples that are not extensively differentiated, and do not contain considerable amounts of accumulated mafic minerals or plagioclase. In all diagrams, the black filled circles labelled "primitive" symbolise the analyses that pass this screening while the grey triangles labelled "differentiated" fail the screening by one or more criteria.

The primitive samples show a clear tholeiitic affinity while the differentiated samples trend into the more calc-alkaline field of the AFM plot (Fig. 6b). The significance of the screening is also visible in the major element variation diagrams in Figure 7 and trace element variation diagrams in Figure 8. The primitive gabbros have higher magnesium numbers in general and tend to form a more concentrated trend. The lower the Mg#, the more variation is seen in element concentration. The La/Lu ratio shows that the primitive gabbros have very little LREE enrichment relative to HREE, which sets them apart from the differentiated samples.

In Figure 7, four analyses are highlighted in red and green. The red ones represent the two dykes lying side by side on outcrop XXI with unclear intrusion order, and the green ones are from outcrop XXV where the plutonic rocks have been emplaced

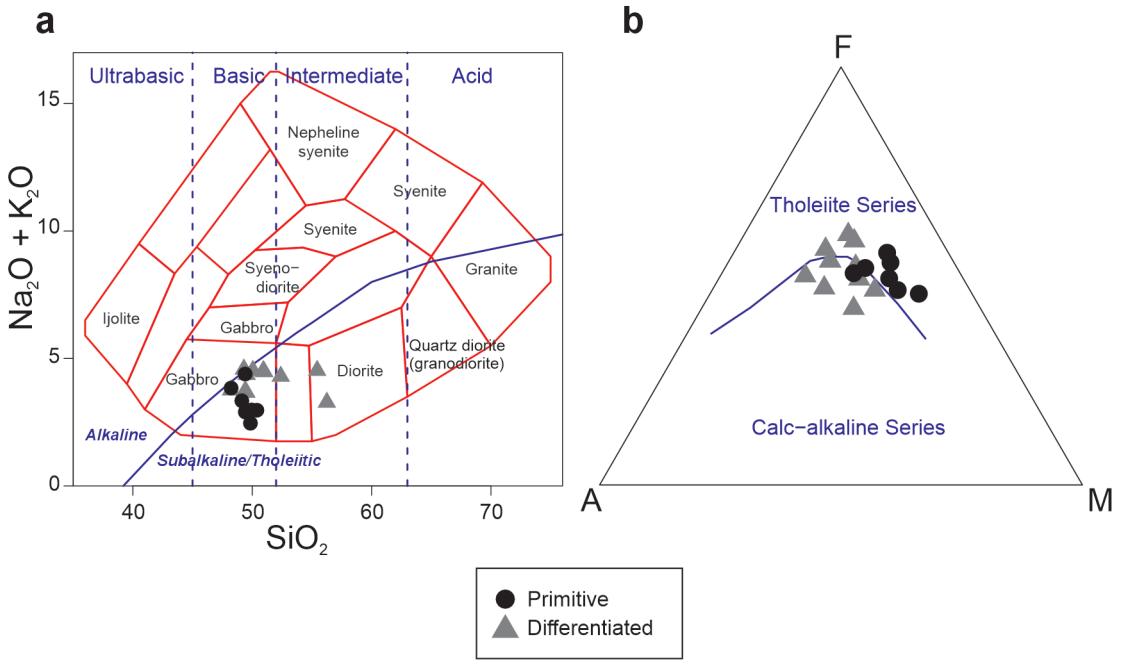

Figure 6. Classification of the Kaiplot gabbros. a) Total alkalis vs. silica (TAS) in wt.% (Cox et al. 1979). b) AFM-plot after Irvine and Baragar (1971) (A = Na_2O + K_2O (alkalis), F = FeO + Fe_2O_3, M = MgO).

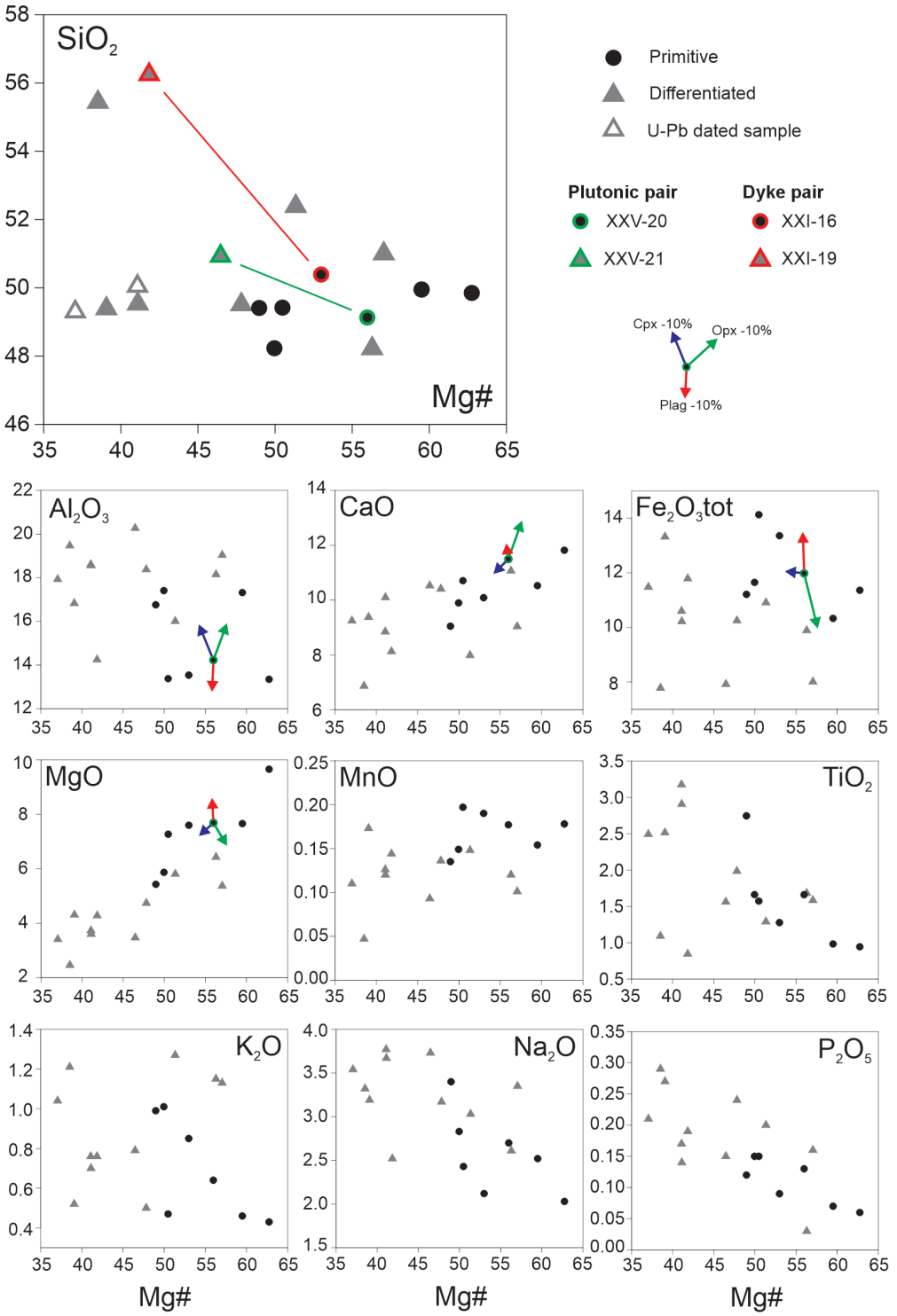

Figure 7. Major element (wt.%) vs Mg# (calculated as 100*(MgO/(FeO+MgO)) [mol.%]). In the SiO_2-diagram the samples marked with red and green represent two intrusive pulses on the same outcrop. The calculated magma evolution arrows represent numerical modelling (removal of 10 % of certain mineral phases) based on whole-rock geochemical data and SEM mineral analysis on sample XXV-20.

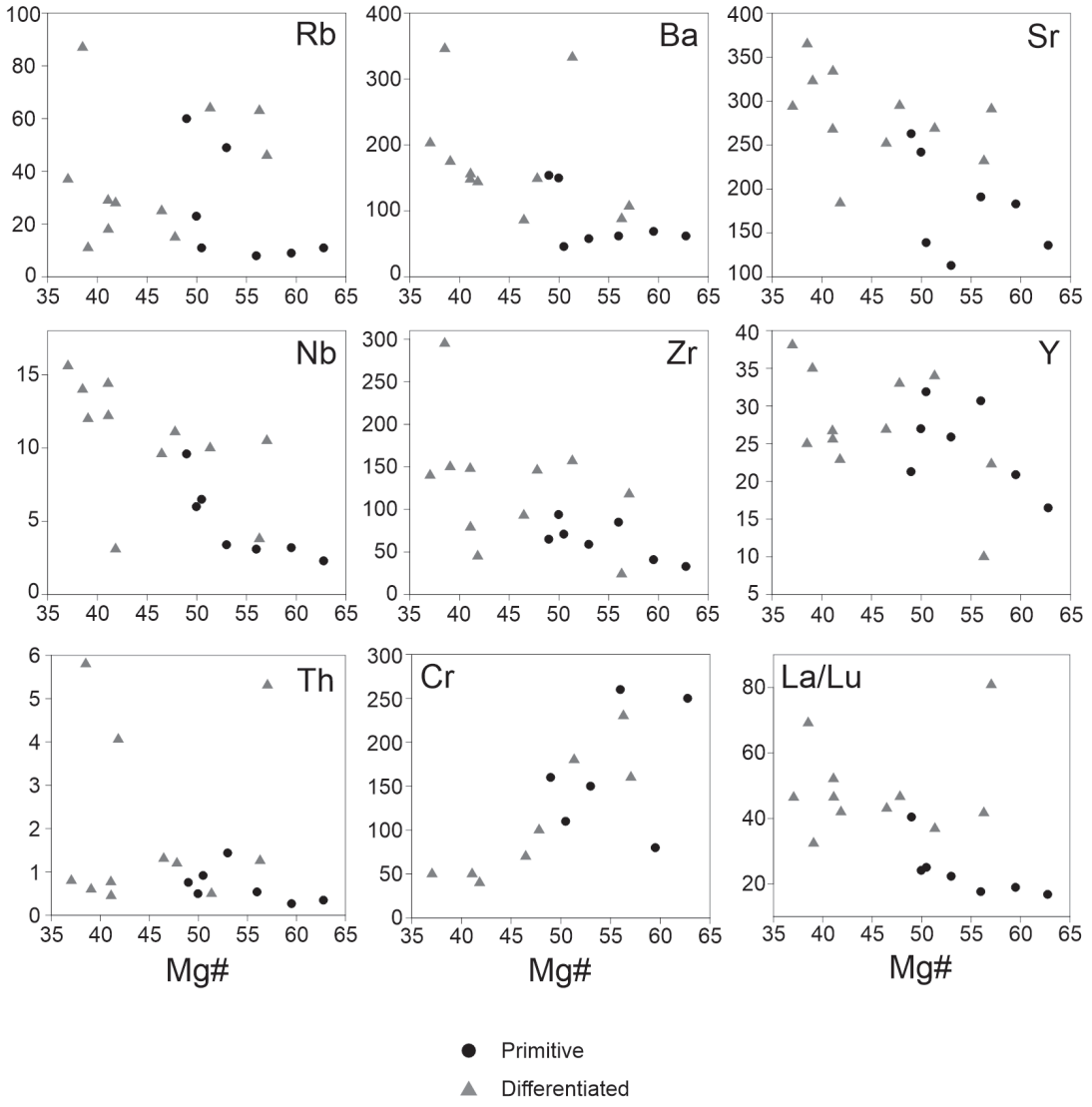

Figure 8. Trace element (ppm) vs Mg# (calculated as 100*(MgO/(FeO+MgO)) [mol.%]).

in two pulses with a clear intrusion order (see Fig. 3a, c). Geochemical analysis shows that the magma composition has changed between the pulses. The pulse represented by sample XXV-21 intruded first, and after it had cooled the second pulse (XXV-20) that is more primitive in composition, was emplaced.

The primitive samples form relatively similar and flat REE patterns in the chondrite-normalised diagram (Fig. 9a). The Eu-anomaly associated with plagioclase accumulation or fractionation is evident in only a few of the most and least enriched samples respectively. The differentiated sample with the lowest REE content and a positive Eu anomaly (XXII) is probably a plagioclase cumulate. In the MORB-normalised trace element diagram, the LILE contents are slightly elevated, but generally less pronounced in the primitive samples compared to the differentiated samples (Fig. 9b).

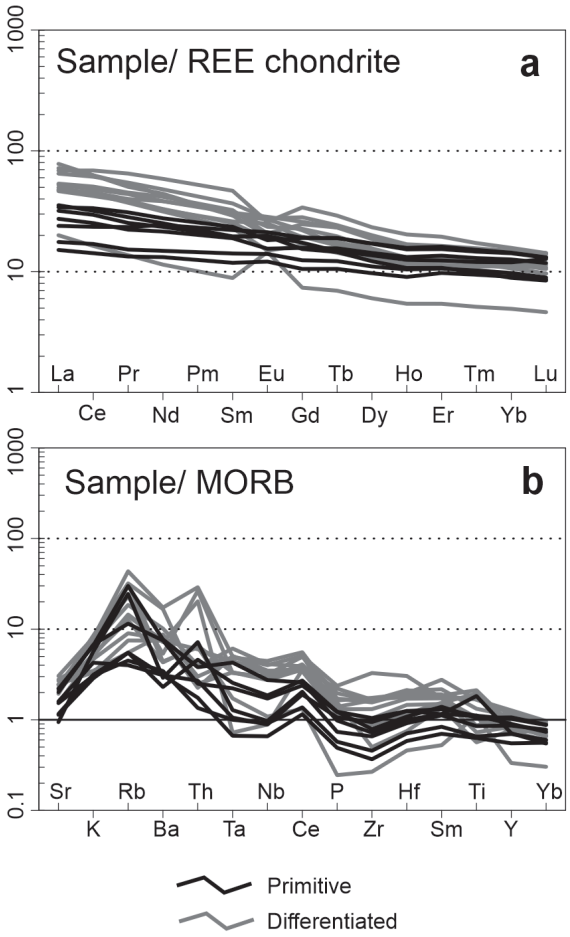

Figure 9. Multielement normalised diagrams of the Kaiplot gabbros. a) Chondrite-normalised REE diagram, normalisation after Boynton (1984). b) MORB-normalised diagram, normalisation and element order after Pearce (1983).

5. Discussion

5.1 Age data

The TIMS dating method that was used on the Kaiplot gabbros has potential to yield mixed ages because several stages/zones of zircon growth inside the grains are analysed together. The relatively high precision of ± 2 Ma of the Kaiplot gabbros implies minimal within-grain variation, and since the analysed zircons come from two different outcrops within the area, the suggested age for the Kaiplot gabbros, 1865 ± 2 Ma, can be considered a reasonable age estimate.

During recent years, an increasing number of mafic rocks in the SFS and south-central Sweden have been dated at the "intraorogenic" stage (see Table 3 and Fig. 10). The majority of the mafic rocks shows ages between 1870 and 1855 Ma. The 1865 ± 2 Ma Kaiplot gabbros fit well into this age group.

5.2 The Kaiplot gabbros in a local context

The Kaiplot gabbros have intruded in several pulses into both brittle and ductile crust. In the initial stages of their emplacement, the surrounding crust is still cold and brittle, but if the magma input is high, the wall rock temperature rises, and partial or complete melting is initiated. The mafic magma and the wall rock melt can then interact to form hybrid magmas if chemically mixed or mingling structures where the mixing is only physical (Huppert & Sparks 1988; Heinonen et al. 2021; Weinberg et al. 2021). Such mingling structures are seen within the Kaiplot area, which implies substantial input of thermal energy from mafic magma to the Svecofennian crust.

Väisänen et al. (2012) described another outcrop of mafic and felsic rocks with similar ages (diorite 1852 ± 4 Ma, granite 1849 ± 8 Ma) in the northern Korpo area less than 20 km west of the Kaiplot area. This mafic intrusion is similarly situated outside of the large recumbent fold system (see Fig. 2a and 10). Our interpretation is that the Korpo diorite and the Kaiplot gabbros belong to a similar tectonic and thermal environment.

The Kaiplot gabbros have been emplaced in an area dominated by porphyritic granite. The porphyritic granites, including the Mattnäs granite and the other microcline granites that are common in the archipelago have in general been considered "lateorogenic" and related to the second folding phase only, but Edelman & Jaanus-Järkkälä (1983) already pointed out

Table 3. Compilation of published ages for extension-related Svecofennian mafic rocks in the Southern Finland and Bergslagen area. See Figure 10 for geographical distribution.

Age, Ma	Location	Type	Reference
1869 ± 8	Ladoga, Puutsaari	gabbro-monzodiorite	Konopelko & Eklund 2003
1868 ± 3	Hakkila, Vantaa	tonalitic dyke	Pajunen et al. 2008
1865 ± 9	Rauma city	diorite	Väisänen et al. 2012
1865 ± 2	Kaiplot, Nagu	gabbro	This study
1863 ± 6	Olkiluoto	tonalitic gneiss	Mänttäri et al. 2006
1861 ± 4	Urjala	high-Mg gabbro (HMG)	Kara et al. 2020
1859 ± 5	Moisio, Turku	monzogabbro	Nevalainen et al. 2014
1859 ± 5	Urjala	high-Nb gabbro (HNB)	Kara et al. 2020
1859 ± 19	Torsholma, Åland	metadiabase dyke	Ehlers et al. 2004
1856 ± 7	Olkiluoto	diabase dyke	Mänttäri et al. 2006
1852 ± 4	Galtby, Korpo	diorite	Väisänen et al. 2012
1870–1850*	Herräng, Bergslagen	amphibolitic dyke	Johansson & Karlsson 2020
1838 ± 4	Jyskelä, Tuusula	gabbro	Pajunen et al. 2008

* Exact age unclear; younger than 1.87 Ga which is the age of the country rock. The metamorphic age (U-Pb, titanite) is 1848 ± 13.

that this model is oversimplified. They state that the granites in the area were probably formed through a number of processes (recrystallisation, metasomatic replacement, anatexis and intrusion) during a prolonged period when the conditions developed into being suitable for granite formation. The published age with large error (1842 ± 31 Ma, Suominen 1991) is the only attempt so far to date the Mattnäs granite. Stålfors & Ehlers (2006) proposed that the granites in the Nagu area have indeed formed as several batches of varying degrees of partial melting, trapped and spread out under a roof of overturned amphibolites. The melts were produced separately during a prolonged time and squeezed out of the protolith by shearing.

5.3 Magma differentiation and origin

The calculated bulk magma evolution shown for a selected number of major elements in Figure 7 implies that the fractionation of clinopyroxene is the major driver of magma evolution. Both major and trace element distributions (Fig. 7 and 8) vary much more for the differentiated samples. This is evident especially for the incompatible elements enriched in the continental crust, such as K_2O, Zr, Rb, Ba, Sr, Th and LREE.

To compare the influence of crystal fractionation versus assimilation of wall rock, we performed simple AFC modelling (DePaolo 1981) on the Kaiplot gabbro data. The surrounding porphyritic granite was used as wall rock contaminant (data from Stålfors & Ehlers 2006). Since clinopyroxene has the most influence on the fractionation, the AFC modelling is simplified not taking other mineral phases into account. As seen in Figure 11, some of the samples, especially the more primitive ones, follow the modelled trend for pure fractionation, while others better resemble the curves for different degrees of wall rock assimilation. Accordingly, the Kaiplot gabbros have likely been subjected to both crystal fractionation and assimilation of wall rock material during differentiation.

Geochemical diagrams used to interpret magma type and tectonic setting are based on relatively recent volcanic rock types (Rollinson 1993). The plate tectonic processes were likely somewhat different during the Paleoproterozoic due to higher crustal and mantle temperatures. Therefore, some

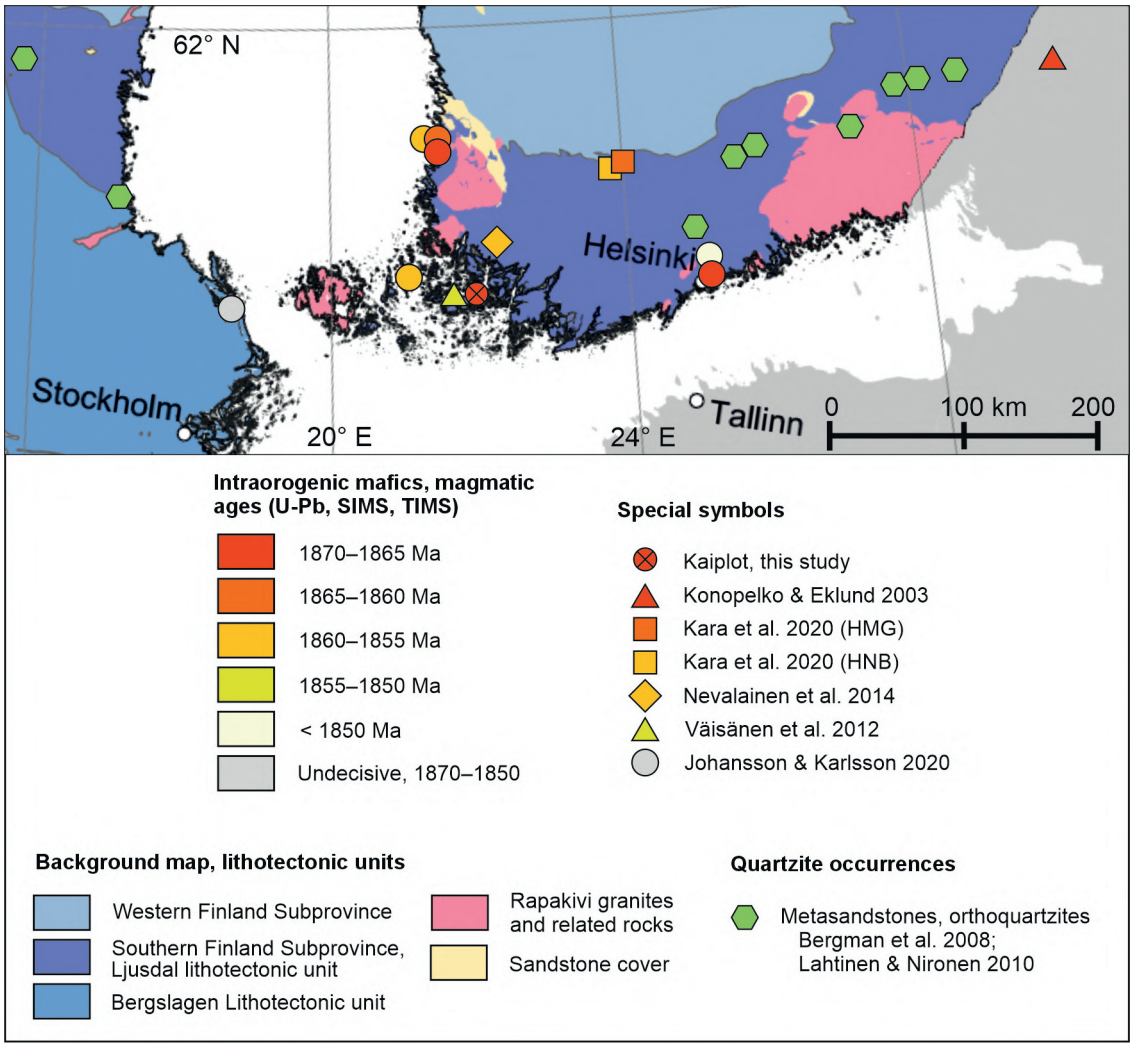

Figure 10. Extension-related Svecofennian mafic intrusions together with quartzite occurrences. See Table 3 for reference information. Background map adopted from Lithotectonic map of Fennoscandia (Luth et al. 2024).

caution is needed when interpreting tectonic discrimination diagrams for older rocks.

The triangular La-Y-Nb diagram of Cabanis & Lecolle (1989) was constructed to discriminate between volcanic arc basalts, continental basalts, and oceanic basalts (Fig. 12). The Kaiplot gabbros are compared with data for other mafic rocks of similar ages (see Figure 10 and Table 3). The primitive Kaiplot samples plot in and around the field for back-arc basin basalt (BABB) which is compatible with an extensional tectonic setting. The more differentiated Kaiplot gabbros and most of the other samples plot into domains representing compressional tectonics which likely reflects higher input of crustal material.

In the chondrite-normalised REE diagram of Boynton (1984) (Fig. 9a), the primitive samples exhibit relatively flat patterns which suggests a high degree of melting and/or a depleted mantle protolith. The differentiated samples show more pronounced enrichment of LREE over HREE and a larger internal variation, including both positive and negative Eu-anomalies. In the MORB-normalised multielement diagram (Pearce 1983) (Fig. 9b), a negative Ta-Nb anomaly and enrichment in LILE are clear in all samples.

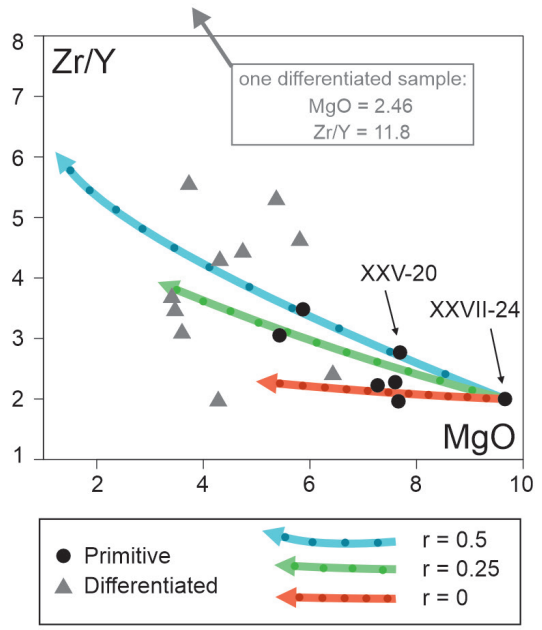

Figure 11. AFC modelling (DePaolo 1981) of the Kaiplot gabbros in an MgO (wt.%) vs Zr/Y diagram. Wall rock contaminant: average of the porphyritic granite from northern Nagu (Stålfors & Ehlers 2006). The dots on the coloured AFC curves represent F values (remaining liquid fraction) where XXVII-24 represents parental magma (F = 1) and each subsequent dot a step of -0.05, the ones furthest to the left representing F = 0.45. The proportion of assimilation vs fractionation is expressed as the r value, where r = 0 is pure fractionation. Partition coefficients in clinopyroxene used in the calculations: MgO = 1.72; Zr = 0.26; Y = 0.412 (that of MgO calculated from SEM pyroxene analysis (see Electronic Appendix A) and whole-rock data from sample XXV-20, and those for Zr and Y taken from the PELE database (Boudreau 1999)).

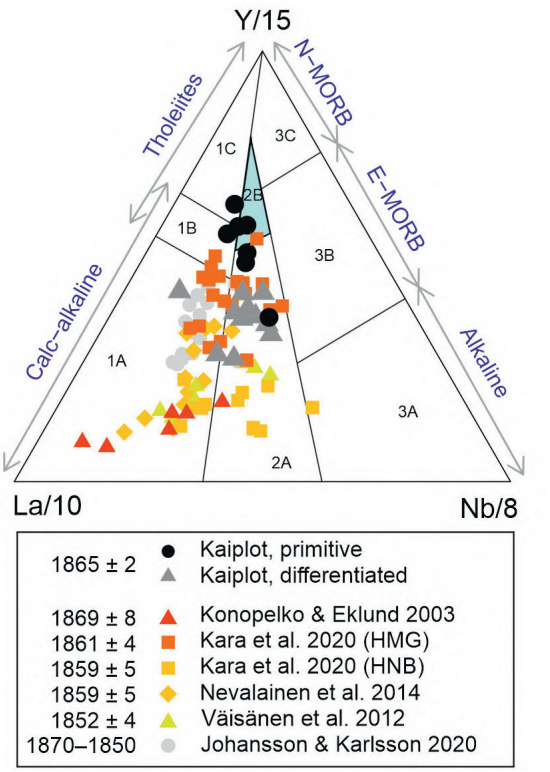

Figure 12. Triangular diagram by Cabanis & Lecolle (1989). The primitive Kaiplot gabbros plot in and around the BABB field (highlighted in blue) in the corner for tholeiitic magmas. The fields are as follows: 1. Volcanic arc basalts (1A = calc-alkaline basalts, 1B = overlap, 1C = volcanic arc tholeiites); 2. Continental basalts (2A = continental basalts, 2B = back-arc basin basalts); 3. Oceanic basalts (3A = alkali basalts/intercontinental rifts, 3B = E-MORB, 3C = N-MORB).

These indicate that some subduction-related contaminants and/or mantle protoliths have been involved in the magma formation (see, e.g., McCulloch & Gamble 1991; Stolz et al. 1996).

Another attempt to trace the source for the Kaiplot gabbros and other related rocks is shown in Figure 13. The diagram is based on the distribution of certain trace elements between the melt and solid fraction when mantle peridotites of different mineral composition (indicating depth) is subjected to partial melting to various degrees. The overall trend for the whole dataset of extension-related Svecofennian mafic rocks goes from a low degree of partial melting of a more garnet-rich, i.e. deep-seated, mantle source towards a higher degree of melting of spinel-bearing shallower mantle. The primitive Kaiplot samples represent the most depleted magma type, i.e. the highest degree of partial melting of a shallow mantle. The differentiated Kaiplot samples and the other related rocks represent processes such as emplacement through thicker crust or a source that is more fertile, possibly enriched by subduction.

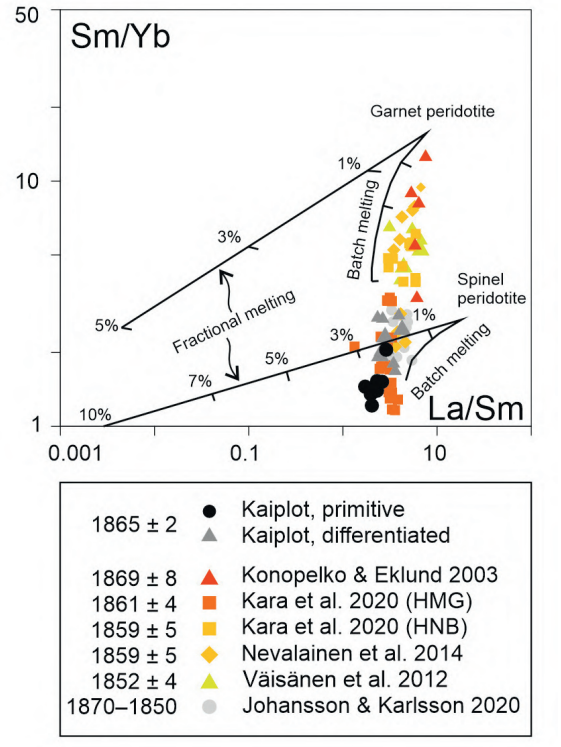

Figure 13. REE data from Kaiplot and other mafics of the same age group compared to modelled mantle melting curves adopted from Genç & Tüysüz (2010). The data forms a trend between a higher degree of partial melting of shallow spinel-bearing mantle and lower degree melting of a garnet-bearing deeper mantle.

5.4 *Interpretation and implication for the Svecofennian crustal evolution*

The Kaiplot gabbros have intruded in several pulses with varying geochemistry. On outcrop XXV where two pulses are discernible, their geochemistry suggests a development from a slightly enriched/differentiated towards a more depleted magma type. Figure 14 illustrates our model for the emplacement of the Kaiplot gabbro dykes and plutons. In the initial rifting phase, the magma was more enriched, partly because it might have originated from a low degree of partial melting of a deeper garnet-bearing mantle, possibly with a subduction-enriched composition, and partly due to a higher degree of differentiation. When the rift system matured due to mantle upwelling, the lithospheric mantle and the crust successively became thinner and more ductile. The associated gabbroic magmas were created by higher degrees of partial melting of shallower spinel-bearing mantle. Large plutonic bodies that conducted enough thermal energy to melt the surrounding country rock were formed. The mafic intrusive magma mingled with the anatectic felsic crustal melts. For comparison, Cui et al. (2020) describe a back-arc system of Devonian age on the border between Mongolia and Kazakhstan. They assume that rocks emplaced in the initial stages of the back-arc rifting more likely show trace-element patterns that are relatively more enriched and resemble island arcs. This is due to greater input of subduction-related crustal material and possibly also because the initial melts may have originated by lower degree of partial melting at a greater depth. When the back-arc rifting system matures and widens, the crustal input decreases and magma compositions approach E-MORB and N-MORB as the main magma source evolves towards a higher degree of partial melting of shallow depleted mantle.

Age determinations from Kaiplot and the reference data show that the mafic rocks were emplaced between 1868 Ma and ca 1840 Ma, the majority of them during the earliest 20 million years of this timespan (Table 3, Fig. 10). There is no clear pattern or consistency between these intrusions regarding age, magma composition or geotectonic environment (Fig. 10, 12 and 13). These intrusions are spread over a large area, and the magmas are diverse. This was probably not a simple extension that deepened and widened linearly, but a process that was fragmented and discontinuous, as well as interrupted early before any oceanic crust was formed. Magni et al. (2021) have done numerical modelling on the complex development of back-arc systems. They conclude that discontinuous extension can be caused by episodic trench retreat, and more generally by changes in subduction dynamics. This leads to asymmetry as multiple basins can develop due to the occurrence of rift

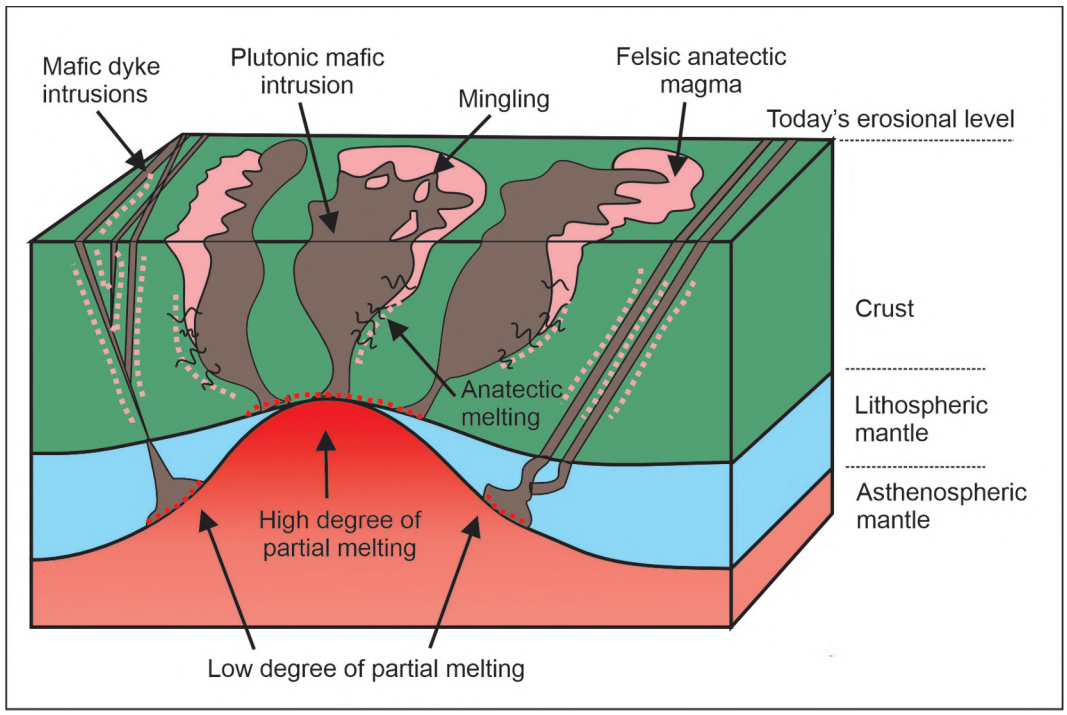

Figure 14. Simplified sketch of the generation of the Kaiplot gabbro intrusions, dykes and plutons (not to scale). In the initial rifting phase, the magma intrudes as fissure dykes into brittle crust. When the rifting matures, the crust is heated and becomes more ductile. Plutons are emplaced and mingle with partially molten crust locally.

and/or ridge jumps. The duration of the initial extensional phase is the most important parameter that controls the distance of and time interval between rift/ridge jumps, and hence the structure and (a-)symmetry of the basin. If the initial extensional episode continues for a longer time, the basin formed is large enough to concentrate further rifting to the same or a nearby location. Shorter episodes of rifting cause multiple basins to form via irregular rift jumps which allow several sedimentary basins with interspersed magmatism between continental fragments. Magni et al. (2021) also point out that magmatism is not only active during phases of extension, but gradually increases and decreases from one extensional episode and location to another, with different geochemical fingerprints as a result.

We think that this is what could have happened in the SFS during the Svecofennian orogeny between 1.87 and 1.84 Ga. The initiation of episodic rifting can be the result of a retreating subduction zone in a setting of tectonic switching as described in the model by Hermansson et al. (2008). During slab retreat the terrain is extended causing splitting of the crust and formation of microcontinent slivers.

Kara et al. (2021) suggested that the Tampere, Pirkanmaa and Häme belts at the northern border and parts of the SFS (Fig. 1) were subjected to alternating extension and contraction due to hinge retreat/advance of a single subducting slab with constant polarity. They present a model of the magmatic evolution in these belts from 1.92 to 1.86 Ga that consists of tectonic switching where the extensional foci successively shift southwards through the back-arc and fore-arc areas of the vaguely defined arc terrains. At 1.86 Ga, the extension-related magmatism waned in the northern belts, but may already have been active in the Uusimaa belt further south. Hermansson et al. (2008) argue that tectonic switching is the predominant model for the bedrock formation of

south-central Sweden, while the preferred tectonic model for the Southern Finland Subprovince is the one with island arcs and microcontinent collisions (Nironen 2017; Lahtinen et al. 2023 and others).

Presented alternative models include melting and migmatisation in the LSGM zone by redistribution of radiogenic heat (from U, Th and K) within tectonically stacked terrains (Kukkonen & Lauri 2009) and an extensional event by gravitational collapse between the two collisional events at ca 1.89–1.87 Ga and 1.84–1.81 Ga (Korja & Heikkinen 2005; Lahtinen et al. 2009). Neither of the models involve major mantle-derived magmatism.

We argue that the Southern Finland Subprovince can be interpreted as a continental back-arc complex with multiple intrusion foci due to rift jumps, which would explain different geochemical fingerprints for the mafic magmatism in the area. Several dyke intrusions observed in the field suggest extensional episodes with mantle-derived magmatism. Compared to the reference data, the Kaiplot gabbros geochemically represent the most mature phase of this extension process with the most BABB-like signatures recognised so far. The area in question is characterised by the LSGM zone (Ehlers et al. 1993), a belt of migmatites, anatectic granites and bimodal magmatism, metamorphosed in amphibolite to granulite facies. In the same area, quartz-rich metasandstone units are documented (Bergman et al. 2008; Lahtinen & Nironen 2010). Stratigraphical data and age data from detrital zircons indicate that the original quartz-rich sediments were deposited in several sedimentary basins that had formed between the two Svecofennian collisional episodes, i.e. ca 1.87–1.84 Ga ago.

We suggest that the tectonic switching model by Collins (2002), applied to the Svecofennian orogeny by Hermansson et al. (2008), has capacity to explain many of the characteristics of the SFS. The Svecofennian orogen is probably a combination of a number of accreting microcontinents, a withdrawing subduction zone with alternating compressional and extensional cycles and gravitational collapse of local hot orogenic belts. Putting this into a bigger context with larger craton systems moving in respect to each other during the Paleoproterozoic will shed further light on the mechanisms and terrain distributions (see, e.g., Bogdanova et al. 2015; Mints et al. 2020; Johansson et al. 2022; Lahtinen et al. 2022, 2023), but this is outside the scope of this paper.

6. Conclusions

In this paper, we describe the field relations, petrography, age and whole-rock major and trace element geochemistry of the Kaiplot gabbros in Nagu (Nauvo), SW Finland. The intrusions are situated in the LSGM zone in the SFS. Our main findings and interpretations can be summarised as follows:

- The Kaiplot gabbros occur as both plutons and dykes with varying grain sizes. The main plutonic body is a hornblende gabbronorite. Formation of wall-rock melts is manifested by mingling structures.
- U-Pb dating of zircon (TIMS) gives an age of 1865 ± 2 Ma, which allows time correlation with the previously suggested "intraorogenic" stage of the Svecofennian orogeny.
- Geochemically the most primitive Kaiplot gabbros show BABB/tholeiitic extension-related affinities. Their parental magmas appear to have originated from relatively high-degree partial melting of shallow mantle. The more differentiated Kaiplot magmas have probably assimilated more wall rock material than the primitive ones and show more arc-like affinities.
- Reference data from mafic rocks of similar age from southern Finland and the Bergslagen area suggest extension-related magmatism with geochemical signatures shifting from volcanic arc to BABB, which is characteristic for back-arc magmatism. Among these rocks, the Kaiplot gabbros exhibit the most pronounced BABB affinities.

We consider alternating phases of extension and compression (tectonic switching) as the most likely explanation for the Svecofennian mafic magmatism between 1.87 and 1.84 Ga.

Acknowledgements

The first author thanks Professor Emeritus Carl Ehlers for introducing her to the subject and Tom Stålfors for valuable field work company. Laboratory engineer Sören Fröjdö assisted with the SEM analysis and data handling. The thin sections were prepared at the Geohouse in Turku by laboratory technician Arto Peltola. The U-Pb-dating was performed by Irmeli Mänttäri at GTK, Espoo. The authors are grateful for the critical and constructive comments by the reviewers J. Pownall and R. Lahtinen and for clear instructions from the editors J. Kohonen and A. Luttinen. This project was financially supported by the Åbo Akademi University Graduate School.

Authorship contribution statement

A. E. Johnson – sampling, sample preparation, writing, analytical work, data curation, modelling, visualisation, background, interpretation, editing; O. Eklund – conceptualisation, interpretation, editing; J. S. Heinonen – editing, interpretation, conceptualisation.

Supplementary data

Electronic Appendix A for this article is available via Bulletin of the Geological Society of Finland web page.

References

Bergman, S., Högdahl, K., Nironen, M., Ogenhall, E., Sjöström, H., Lundqvist, L. & Lahtinen, R., 2008. Timing of Palaeoproterozoic intra-orogenic sedimentation in the central Fennoscandian Shield; evidence from detrital zircon in metasandstone. Precambrian Research 161, 231–249. https://doi.org/10.1016/j.precamres.2007.08.007

Bogdanova, S., Gorbatschev, R., Skridlaite, G., Soesoo, A., Taran, L., Kurlovich, D., 2015. Trans-Baltic Palaeoproterozoic correlations towards the reconstruction of supercontinent Columbia/Nuna. Precambrian Research 259, 5–33. http://dx.doi.org/10.1016/j.precamres.2014.11.023

Boudreau, A. E., 1999. PELE—a version of the MELTS software program for the PC platform. Computers & Geosciences 25, 201–203. https://doi.org/10.1016/S0098-3004(98)00117-4

Boynton, W. V., 1984. Cosmochemistry of the Rare Earth Elements: Meteorite Studies. In: Developments in Geochemistry. 63–114. https://doi.org/10.1016/B978-0-444-42148-7.50008-3

Cabanis, B. & Lecolle, M., 1989. Le diagramme La/10-Y/15-Nb/8: un outil pour la discrimination des séries volcaniques et la mise en évidence des processus de mélange et/ou de contamination crustale. Comptes Rendus de l'Academie de Sciences de Paris série II 309: 2023–2029.

Collins, W. J., 2002. Hot orogens, tectonic switching, and creation of continental crust. Geology 30, 535–538. https://doi.org/10.1130/0091-7613(2002)030<0535:HOTSAC>2.0.CO;2

Cox, K. G., Bell, J. D. & Pankhurst, R. J., 1979. The Interpretation of Igneous Rocks. Allen and Unwin, London. https://doi.org/10.1007/978-94-017-3373-1

Cui, X., Sun, M., Zhao, G., Yao, J., Zhang, Y., Han, Y. & Dai, L., 2020. A Devonian arc–back-arc basin system in the southern Chinese Altai: Constraints from geochemical and Sr-Nd-Pb isotopic data for meta-basaltic rocks. Lithos 366–367. https://doi.org/10.1016/j.lithos.2020.105540

Dahlin, P., Johansson, Å. and Andersson, U. B., 2014. Source character, mixing, fractionation and alkali metasomatism in Palaeoproterozoic greenstone dykes, Dannemora area, NE Bergslagen region, Sweden. Geological Magazine 151, 573–590. https://doi.org/10.1017/S0016756813000551

D'Elia, L., 2010. Caracterización Estratigráfica y Estructural de La Evolución Temprana (Sin-Rift y Post-Rift Inicial) Del Margen Sur de La Cuenca Neuquina Entre Sañicó (Neuquén) y El Río Limay (Río Negro). PhD Thesis, Universidad Nacional de La Plata.

DePaolo, D. J., 1981. Trace element and isotopic effects of combined wallrock assimilation and fractional

crystallization. Earth and Planetary Science Letters 53, 189–202. https://doi.org/10.1016/0012-821X(81)90153-9

Edelman, N., 1972. A Porphyroblastic Granite with Preserved Bedding. Geologiska Föreningens i Stockholm Förhandlingar 94, 193–211. https://doi.org/10.1080/11035897209454197

Edelman, N., 1973. Nagu. Geological map of Finland 1:100 000, pre-Quaternary rocks, sheet 1034, Geological Survey of Finland.

Edelman, N., 1985. Nagu. Explanation to the Geological map of Finland 1:100 000, pre-Quaternary rocks, sheet 1034, 50 p. (in Finnish with Swedish and English summary).

Edelman, N. & Jaanus-Järkkälä, M., 1983. A Plate Tectonic Interpretation of the Precambrian of the Archipelago of Southwestern Finland: With 13 Figures. Geological Survey of Finland, Bulletin 325, 36 p.

Ehlers, C., Lindroos, A. & Jaanus-Järkkälä, M., 1986. Stratigraphy and geochemistry in the proterozoic mafic volcanic rocks of the Nagu-Korpo area, SW Finland. Precambrian Research 32, 297–315. https://doi.org/10.1016/0301-9268(86)90034-3

Ehlers, C., Lindroos, A. & Selonen, O., 1993. The late Svecofennian granite-migmatite zone of southern Finland—a belt of transpressive deformation and granite emplacement. Precambrian Research 64, 295–309. https://doi.org/10.1016/0301-9268(93)90083-E

Ehlers, C., Skiöld, T. & Vaasjoki, M., 2004. Timing of Svecofennian crustal growth and collisional tectonics in Åland, SW Finland. Geological Society of Finland, Bulletin 76, 63–91. https://doi.org/10.17741/bgsf/76.1-2.004

Eklund, O., Konopelko, D., Rutanen, H., Fröjdö, S. & Shebanov, A. D., 1998. 1.8 Ga Svecofennian post-collisional shoshonitic magmatism in the Fennoscandian shield. Lithos 45, 87–108. https://doi.org/10.1016/S0024-4937(98)00027-9

Gaál, G. & Gorbatschev, R., 1987. An outline of the Precambrian evolution of the Baltic Shield. Precambrian research 15–52. https://doi.org/10.1016/0301-9268(87)90044-1

Genç, Ş.C. & Tüysüz, O., 2010. Tectonic setting of the Jurassic bimodal magmatism in the Sakarya Zone (Central and Western Pontides), Northern Turkey: A geochemical and isotopic approach. Lithos 118, p. 95–111. https://doi.org/10.1016/j.lithos.2010.03.017

Hausen, H., 1944. Geologische Beobachtungen im Schärenhof von Korpo-Nagu Südwest-Finnland: mit besonderer Berücksichtigung der Grobgranite und ihrer klufttektonischen Verhältnisse. Meddelanden från Åbo Akademis geologisk-mineralogiska institut.

Heinonen, J. S., Iles, K. A., Heinonen, A., Fred, R., Virtanen, V. J., Bohrson, W. A. & Spera, F. J., 2021. From Binary Mixing to Magma Chamber Simulator: Geochemical Modeling of Assimilation in Magmatic Systems. In: Masotta, M., Beier, C. and Mollo, S. (eds), Geophysical Monograph Series 151–176. https://doi.org/10.1002/9781119564485.ch7

Hermansson, T., Stephens, M.B., Corfu, F., Page, L.M. & Andersson, J., 2008. Migratory tectonic switching, western Svecofennian orogen, central Sweden: Constraints from U/Pb zircon and titanite geochronology. Precambrian Research 161, 250–278. https://doi.org/10.1016/j.precamres.2007.08.008

Hietanen, A., 1975. Generation of potassium-poor magmas in the northern Sierra Nevada and the Svecofennian of Finland. Journal of Research of the U.S. Geological Survey. 3, 631–645.

Högdahl, K., Andersson, U. B. & Eklund, O. (eds)., 2004. The Transscandinavian Igneous Belt (TIB) in Sweden: A Review of Its Character and Evolution. Geological Survey of Finland, Special paper 37.

Högdahl, K. & Bergman, S., 2020. Chapter 5: Paleoproterozoic (1.9–1.8 Ga), syn-orogenic magmatism and sedimentation in the Ljusdal lithotectonic unit, Svecokarelian orogen. Geological Society, London, Memoirs 50, 131–153. https://doi.org/10.1144/M50-2016-30

Hughes, C. J., 1972. Spilites, keratophyres, and the igneous spectrum. Geological Magazine 109, 513–527. https://doi.org/10.1017/S0016756800042795

Huppert, H. E. & Sparks, R. S. J., 1988. The Generation of Granitic Magmas by Intrusion of Basalt into Continental Crust. Journal of Petrology 29, 599–624. https://doi.org/10.1093/petrology/29.3.599

Irvine, T. N. & Baragar, W. R. A., 1971. A Guide to the Chemical Classification of the Common Volcanic Rocks. Canadian Journal of Earth Sciences 8, 523–548. https://doi.org/10.1139/e71-055

Johansson, Å. & Karlsson, A., 2020. The "intraorogenic" Svecofennian Herräng mafic dyke swarm in east-central Sweden: age, geochemistry and tectonic significance. GFF 142, 1–22. https://doi.org/10.1080/11035897.2019.1708450

Johansson, Å., Bingen, B., Huhma, H., Waight, T., Vestergaard, R., Soesoo, A., Skridlaite, G., Krzeminska, E., Shumlyanskyy, L., Holland, M. E., Holm-Denoma, C., Teixeira, W., Faleiros, F. M., Ribeiro, B. V., Jacobs, J., Wang, C., Thomas, R. J., Macey, P. H., Kirkland, C. L., Hartnady, M. I. H., Eglington, B. M., Puetz, S. J. & Condie, K. C., 2022. A geochronological review of magmatism along the external margin of Columbia and in the Grenville-age orogens forming the core of Rodinia. Precambrian Research, 371. https://doi.org/10.1016/j.precamres.2021.106463

Kähkönen, Y., 2005. Chapter 8 Svecofennian supracrustal rocks. In: Lehtinen, M., Nurmi, P. A. and Rämö, O. T. (eds), Precambrian Geology of Finland - Key to the Evolution of the Fennoscandian Shield, 343–405. https://doi.org/10.1016/S0166-2635(05)80009-X

Kara, J., Väisänen, M., Heinonen, J. S., Lahaye, Y., O'Brien, H. & Huhma, H., 2020. Tracing arclogites in the Paleoproterozoic Era – A shift from 1.88 Ga calc-alkaline

to 1.86 Ga high-Nb and adakite-like magmatism in central Fennoscandian Shield. Lithos 372–373. https://doi.org/10.1016/j.lithos.2020.105663

Kara, J., Leskelä, T., Väisänen, M., Skyttä, P., Lahaye, Y., Tiainen, M. & Leväniemi, H., 2021. Early Svecofennian rift-related magmatism: Geochemistry, U-Pb-Hf zircon isotope data and tectonic setting of the Au-hosting Uunimäki gabbro, SW Finland. Precambrian Research 364. https://doi.org/10.1016/j.precamres.2021.106364

Kohonen, J., Köykkä, J & Mikkola, P., 2024. Stratigraphy of precambrian rocks in finland: a review with emphasis on the application of lithodemic units, regional chronostratigraphic nomenclature and map database management. In: Köykkä, J., Ojala, A. E. K. & Tarvainen, T. (eds), Geological Survey of Finland, Bulletin 418, pp 6–36, 2024. https://doi.org/10.30440/bt418.1

Koistinen, T., Stephens, M. B., Bogatchev, V., Nordgulen, Ø., Wennerström, M. & Korhonen, J., 2001. Geological map of the Fennoscandian Shield 1:2 000 000. Trondheim: Geological Survey of Norway, Uppsala: Geological Survey of Sweden, Moscow: Ministry of Natural Resources of Russia, Espoo: Geological Survey of Finland.

Konopelko, D. & Eklund, O., 2003. Timing and geochemistry of potassic magmatism in the eastern part of the Svecofennian domain, NW Ladoga Lake Region, Russian Karelia. Precambrian Research 120, 37–53. https://doi.org/10.1016/S0301-9268(02)00141-9

Korja, A. & Heikkinen, P., 2005. The accretionary Svecofennian orogen—insight from the BABEL profiles. Precambrian Research 136, 241–268. https://doi.org/10.1016/j.precamres.2004.10.007

Krogh, T. E., 1973. A low-contamination method for hydrothermal decomposition of zircon and extraction of U and Pb for isotopic age determinations. Geochimica et Cosmochimica Acta 37, 485–494. https://doi.org/10.1016/0016-7037(73)90213-5

Krogh, T. E., 1982. Improved accuracy of U-Pb zircon ages by the creation of more concordant systems using an air abrasion technique. Geochimica et Cosmochimica Acta 46, 637–649. https://doi.org/10.1016/0016-7037(82)90165-X

Kukkonen, I. & Lauri, L., 2009. Modelling the thermal evolution of a collisional Precambrian orogen: High heat production migmatitic granites of southern Finland. Precambrian Research 168, 233–246. https://doi.org/10.1016/j.precamres.2008.10.004

Lahtinen, R., Korja, A. & Nironen, M., 2005. Chapter 11 Paleoproterozoic tectonic evolution. In: Lehtinen, M., Nurmi, P. A. and Rämö, O. T. (eds), Precambrian Geology of Finland – Key to the Evolution of the Fennoscandian Shield, pp. 481–531. https://doi.org/10.1016/S0166-2635(05)80012-X

Lahtinen, R., Korja, A., Nironen, M. & Heikkinen, P., 2009. Palaeoproterozoic accretionary processes in Fennoscandia. Geological Society, London, Special Publications 318, pp. 237–256. https://doi.org/10.1144/SP318.8

Lahtinen, R. & Nironen, M., 2010. Paleoproterozoic lateritic paleosol–ultra-mature/mature quartzite–meta-arkose successions in southern Fennoscandia—intra-orogenic stage during the Svecofennian orogeny. Precambrian Research 183, 770–790. https://doi.org/10.1016/j.precamres.2010.09.006

Lahtinen, R., Salminen, P. E., Sayab, M., Huhma, H., Kurhila, M. & Johnston, S.T., 2022. Age and structural constraints on the tectonic evolution of the Paleoproterozoic Saimaa orocline in Fennoscandia. Precambrian Research 369. https://doi.org/10.1016/j.precamres.2021.106477

Lahtinen, R., Köykkäa, J., Salminen, J., Sayab, M. & Johnston, S. T., 2023. Paleoproterozoic tectonics of Fennoscandia and the birth of Baltica. Earth-Science Reviews 246. https://doi.org/10.1016/j.earscirev.2023.104586

Levin, T., Engström, J., Lindroos, A., Baltybaev, S. & Levchenkov, O., 2005. Late-Svecofennian transpressive deformation in SW Finland—evidence from late-stage D_3 structures. GFF 127, pp. 129–137. https://doi.org/10.1080/11035890501272129

Ludwig, K. R., 1991. PbDat 1.21 for MS-dos: A computer program for IBM-PC Compatibles for processing raw Pb-U-Th isotope data. Version 1.07.

Ludwig, K. R., 2003. User's manual for Isoplot/Ex version 3.00, a geochronological toolkit for Microsoft Excel. Berkeley Geochronology Center Special Publications, 72 pp.

Luth, S. W., Torgersen, E. & Köykkä, J., 2024. Lithotectonic map of Fennoscandia. Conference poster, 36th Nordic Geological Winter Meeting, Gothemburg. https://doi.org/10.13140/RG.2.2.20487.37285

Magni, V., Naliboff, J., Prada, M. & Gaina, C., 2021. Ridge Jumps and Mantle Exhumation in Back-Arc Basins. Geosciences 11, 475. https://doi.org/10.3390/geosciences11110475

Mänttäri, I., Talikka, M., Paulamäki, S. & Mattila, J., 2006. U-Pb Ages for Tonalitic Gneiss, Pegmatitic Granite, and Diabase Dyke, Olkiluoto Study Site, Eurajoki, SW Finland. Technical Report, Posiva.

McCulloch, M. T. & Gamble, J. A., 1991. Geochemical and geodynamical constraints on subduction zone magmatism. Earth and Planetary Science Letters, 102 (3-4), pp. 358–374. https://doi.org/10.1016/0012-821X(91)90029-H

Mints, M. V., Glaznev, V. N., Muravina, O. M. & Sokolova, E. Y., 2020. 3D model of Svecofennian Accretionary Orogen and Karelia Craton based on geology, reflection seismics, magnetotellurics and density modelling: Geodynamic speculations. Geoscience Frontiers, 11, issue 3, pp. 999–1023. https://doi.org/10.1016/j.gsf.2019.10.003

Nevalainen, J., Väisänen, M., Lahaye, Y., Heilimo, E. & Fröjdö, S., 2014. Svecofennian intra-orogenic gabbroic magmatism: A case study from Turku, southwestern Finland. Geological Society of Finland, Bulletin 86, pp. 93–112. https://doi.org/10.17741/bgsf/86.2.003

Nironen, M., 2005. Chapter 10 Proterozoic orogenic granitoid rocks. In: Lehtinen, M., Nurmi, P. A. and Rämö, O. T. (eds), Precambrian Geology of Finland – Key to the Evolution of the Fennoscandian Shield, pp. 443–479. https://doi.org/10.1016/S0166-2635(05)80011-8

Nironen, M., 2017. Guide to the Geological Map of Finland – Bedrock 1:1 000 000. Geological Survey of Finland, Special Paper 60, pp. 41–76.

Pajunen, M., Airo, M-L., Elminen, T., Mänttäri, I., Niemelä, R., Vaarma, M., Wasenius, P. & Wennerström, M., 2008. Tectonic evolution of the Svecofennian crust in southern Finland. In: Pajunen, M. (ed.), Tectonic evolution of the Svecofennian crust in southern Finland - a basis for characterizing bedrock technical properties. Geological Survey of Finland, Special Paper 47, pp. 15–160.

Pearce, J., 1983. The role of subcontinental lithosphere in magma genesis at destructive plate margins. Philosophical Transactions of the Royal Society of London 317, pp. 253–266.

Ramsay, W., 1912. Geologiens grunder II, Översikt av den geologiska utvecklingen, Fennoskandiens Geologi, Andra upplagan.

Rollinson, H. R., 1993. Using Geochemical Data: Evaluation, Presentation, Interpretation. Geochemistry series, Taylor & Francis.

Rutanen, H., Andersson, U. B., Väisänen, M., Johansson, Å., Fröjdö, S., Lahaye, Y. & Eklund, O., 2011. 1.8 Ga magmatism in southern Finland: strongly enriched mantle and juvenile crustal sources in a post-collisional setting. International Geology Review 53, pp. 1622–1683. https://doi.org/10.1080/00206814.2010.496241

Sederholm, J. J., 1926. On Migmatites and Associated Pre-Cambrian Rocks of Southwestern Finland: Part II: The Region Around the Barösundsfjärd W. of Helsingfors and Neighbouring Areas. Bulletin de la Commission géologique de Finlande.

Simonen, A., 1980. The Precambrian in Finland. Geological Survey of Finland, Bulletin 304.

Skyttä, P. & Mänttäri, I., 2008. Structural setting of late Svecofennian granites and pegmatites in Uusimaa Belt, SW Finland: Age constraints and implications for crustal evolution. Precambrian Research 164, pp. 86–109. https://doi.org/10.1016/j.precamres.2008.04.001

Stacey, J. S. & Kramers, J. D., 1975. Approximation of terrestrial lead isotope evolution by a two-stage model. Earth and Planetary Science Letters 26, pp. 207–221. https://doi.org/10.1016/0012-821X(75)90088-6

Stålfors, T. & Ehlers, C., 2006. Emplacement mechanisms of late-orogenic granites: structural and geochemical evidence from southern Finland. International Journal of Earth Sciences 95, pp. 557–568. https://doi.org/10.1007/s00531-005-0049-3

Stephens, M. B. & Andersson, J., 2015. Migmatization related to mafic underplating and intra- or back-arc spreading above a subduction boundary in a 2.0–1.8 Ga accretionary orogen, Sweden. Precambrian Research 264, pp. 235–257. https://doi.org/10.1016/j.precamres.2015.04.019

Stephens, M. B., 2020. Outboard-migrating accretionary orogeny at 1.9–1.8 Ga (Svecokarelian) along a margin to the continent Fennoscandia. In: Stephens, M.B., Bergman Weihed, J. (Eds.), Sweden: Lithotectonic Framework, Tectonic Evolution and Mineral Resources, Geological Society, London, Memoirs, 50, pp. 237–250. https://doi.org/10.1144/M50-2019-18

Stolz, A. J., Jochum, K. P., Spettel, B. & Hofmann, A. W., 1996. Fluid- and melt-related enrichment in the subarc mantle: Evidence from Nb/Ta variations in island-arc basalts. Geology, 24 (7), pp. 587–590. https://doi.org/10.1130/0091-7613(1996)024<0587:FAMREI>2.3.CO;2

Suominen, V., 1991. The Chronostratigraphy of Southwestern Finland with Special Reference to Postjotnian and Subjotnian Diabases. Geological Survey of Finland, Bulletin 356.

Torvela, T., Mänttäri, I. & Hermansson, T., 2008. Timing of deformation phases within the South Finland shear zone, SW Finland. Precambrian Research 160, pp. 277–298. https://doi.org/10.1016/j.precamres.2007.08.002

Väisänen, M. & Hölttä, P., 1999. Structural and metamorphic evolution of the Turku migmatite complex, southwestern Finland. Geological Society of Finland, Bulletin 71, pp. 177–218. https://doi.org/10.17741/bgsf/71.1.009

Väisänen, M., Mänttäri, I. & Hölttä, P., 2002. Svecofennian magmatic and metamorphic evolution in southwestern Finland as revealed by U-Pb zircon SIMS geochronology. Precambrian Research 116, 111–127. https://doi.org/10.1016/S0301-9268(02)00019-0

Väisänen, M., Eklund, O., Lahaye, Y., O'Brien, H., Fröjdö, S., Högdahl, K. & Lammi, M., 2012. Intra-orogenic Svecofennian magmatism in SW Finland constrained by LA-MC-ICP-MS zircon dating and geochemistry. GFF 134, pp. 99–114. https://doi.org/10.1080/11035897.2012.680606

Weinberg, R. F., Vernon, R. H. & Schmeling, H., 2021. Processes in mushes and their role in the differentiation of granitic rocks. Earth-Science Reviews 220. https://doi.org/10.1016/j.earscirev.2021.103665